ON THE PETROLOGY AND EARLY DEVELOPMENT OF THE CRUST OF A MOON OF FISSION ORIGIN*

ALAN B. BINDER

Institut für Geophysik, Neue Universität, Kiel, Bundesrepublik Deutschland

(Received 7 January, 1975)

Abstract. It is proposed that the primitive suite of upland rocks formed as a result of the cumulation of plagioclase which crystallized in disequilibrium from a convecting magma containing previously crystallized and co-crystallizing olivine and pyroxene. As the plagioclase was removed from this magma by flotation, it carried with it melt and mafic crystals in varying, but predictable proportions. This model successfully accounts for the major petrological characteristics of the upland suite of rocks, in particular, the reversed An vs Mg′ trend, the quartz normative anorthosites and the olivine to pyroxene ratio variations vs plagioclase content of the rocks.

It is shown that the crystallization sequence for the Moon is one where the pyroxenes of the peridotite upper mantle and crust were formed as a result of the reaction olivine + quartz (melt) → pyroxene. This reaction occurred at depth (100–300 km) in the moon after the dunite lower mantle had formed, but while olivine was still crystallizing at the surface. As a result of this reaction, the crystallization of the last 20% of the Moon took place mainly along the olivine-plagioclase cotectic and not at the olivine-pyroxene-plagioclase peritectic as previously proposed. This crystallization sequence leads directly to an explanation of the fact that olivine rich rocks make up a significant fraction of the crust, despite the presence of a pyroxene dominated upper mantle directly below the crust. Also the reaction olivine + quartz (melt) → pyroxene is exothermic and as such provided heat energy at the bottom of the magma system needed to set it into strong convective motion. As a result, the magma was kept stirred and the olivine and pyroxene in the cooling magma were kept in equilibrium with the melt, thus finally producing the relatively uniform peridotite of the upper mantle.

A refined model for the distribution of U, Th and K in the crust of a pyroline moon is presented. It is demonstrated that the KREEP layer, which formed at the crust-upper mantle interface at the end of the crystallization of the Moon, was quickly destroyed by impact excavation and the upwards migration of the low melting KREEP materials. As a result of these processes the KREEP layer no longer exists in the Moon and all of its components are mixed in the crust. As a result, the crust contains about 80% of the heat producing U, Th and K of the Moon. The predicted values of the concentrations of U, Th and K in the crust based on this model are almost exactly those found for the average upland crust by the orbiting γ-ray experiment. This result not only strongly supports the models proposed in this paper but also supports the suggestion that the mean heat flow of the moon is 13–14 ergs/cm^2/sec, i.e. that predicted for a Moon of fission origin in an earlier paper.

The results and models presented in this paper further support the hypothesis that the Moon is a gravitationally differentiated body which originated by fission from a protoearth.

1. Introduction

In an earlier paper Binder (1975a, 1975b; hereafter referred to as Paper II) presented a model for the development of the primitive crust of the Moon based largely on the differentiation scheme developed for a Moon of fission origin presented in another paper (Binder, 1974a, 1974b; hereafter referred to as Paper I). This model indicates that the reversed relationship between the An contents of the plagioclase and the 100 Mg/(Mg + Fe) ratios of the mafics of the rocks and other characteristics of the upland rocks can be easily explained if the rocks formed by the disequilibrium crystallization and cumulation of plagioclase which trapped varying amounts of melt and mafics from an equilibriated mixture of crystals and liquid under the growing

* Contribution No. 127, Institut für Geophysik, Kiel.

The Moon **15** (1976) 275–314.

crust. A similar model has been developed independently by Wood (1975a, 1975b) who assumes only that the crust developed as a result of the crystallization of a Moon wide, 'well stirred' melt without any inferences to the origin of the Moon.

This paper presents a more detailed description of the crustal developmental model introduced in Paper II and discusses the implications of this model in regard to the composition and differentiation of a pyrolite Moon of fission origin.

2. Basic Considerations

The basic logic, data and assumptions behind the model to be discussed and the development scheme and composition of the differentiated pyrolite Moon models, of which the crustal model is an integral part, are given in Papers I and II. For the sake of brevity, no attempt will be made to summarize all this material. It is assumed that the reader is familiar with these two papers or will read them before attempting to follow the discussions presented here.

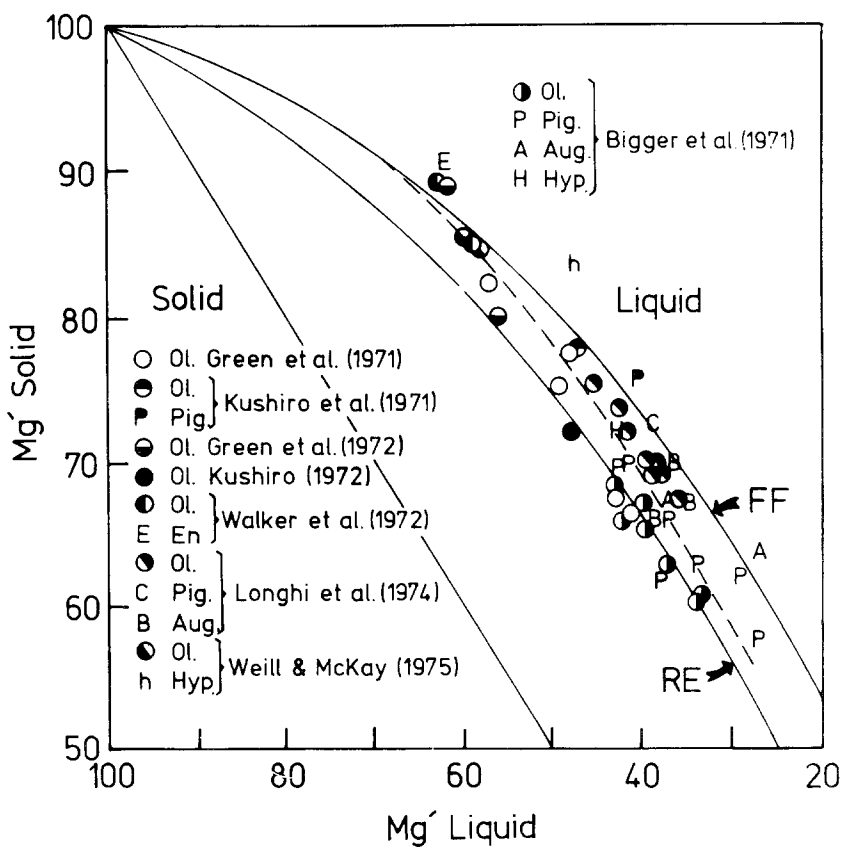

Fig. 1. Pseudo-phase diagrams for olivine and pyroxene. The curves are derived from data by Roeder and Emslie (1970) for olivine (curve RE) and the pure forsterite-fayalite system (curve FF). Included for comparison are data derived from lunar rock experiments. The dashed curve through the experimental points is thought to best represent the liquidus for lunar olivine and pyroxene.

Of the assumptions and data discussed in Papers I and II, several have been slightly revised or updated as follows: First: additional data points giving the 100 Mg/(Mg + Fe) (hereafter refered to as Mg′) ratio of the melt and of the liquids olivine and/or pyroxene have been found (Walker *et al.*, 1972; Longhi *et al.*, 1974; Weill and McKay, 1975) since Paper II was sent to press. As such, Figure 1 of Paper II has been updated and is given as Figure 1 in this paper. The additional points confirm the tentative conclusion derived in Paper II that the liquidus for olivine approaches that of the pure forsterite-fayalite system (FF) at values of Mg′ > 50. The data also show that for Mg′ between 30 and 50, the olivine liquidus lies between that of the FF system and the liquidus defined by Roeder and Emslie (1970). The data also seem to show that there is little difference between the liquidus of olivine and that of pyroxene in the range of Mg′ of interest. As such, the dashed curve in Figure 1 is used to determine the Mg′ contents of the melt and both of these mafic crystals for the various models under study.

Second, based on the discussion given in Section 2 of Paper II, it is assumed that the Moon has retained 20% of the K_2O and Na_2O it originally contained at fission (see Section 4 of Paper I). Thus only 20% retention models are considered in this paper.

Third, the data base of CIPW norms of upland rocks used in these studies has been expanded to some 105 rocks. Table I gives the rock number and source of the data for the rocks added to the data base. The new CIPW norms do not include any for spinel troctolites for the reasons given in Section 5 of Paper II. Also, CIPW

TABLE I

Rocks added to the data base of paper II[a]

References	Rocks
Rose *et al.* (1972)	14047
	14063,37
	14063,46
	14066
	14083 White Clast
	14083 Dark Clast
	14315
	14318
European Consortium (1974)	14267
Dowty *et al.* (1972)	15362
Hubbard *et al.* (1974)	60095
Rose *et al.* (1973)	60017
	60025
	67115
	67455
	68416
	69935
	99955
Duncan *et al.* (1973)	61016
	66095
	67016
	67915,53D
	67915,53L

(*continued*)

Table I (continued).

Reference	Rocks
Dowty *et al.* (1974b)	60516
	60619
	60629
	60659
	60665
	60677
	62275
	65326
	65757
	65767
	65799
Hubbard *et al.* (1973)	63545
Grieve *et al.* (1974)	65702 Clast 2
Taylor *et al.* (1974)	60016
	61175
	62255
	64435
	67016
Taylor *et al.* (1974)	68115
	72275 Poikilitic
	73235 White
	73235 Black
	76315
Stoeser *et al.* (1974a)	72275 Dark Breccia Clast
	72275 Anorthosite Clast
Stoeser *et al.* (1974b)	72275 Anorthosite Clast No. (5)
	72275 Norite Clast
Bence *et al.* (1975)	73215,94 Clast
	73215,94 Matrix
	73215,49
	73215 Average Matrix
Hubbard *et al.* (1974)	76315
Chao and Minkin (1974)	77075
	77115,10-3
	77115,9-1 Poikilitic

[a] See Table X of Paper II

norms for melt rocks (e.g. Dowty *et al.*, 1974a) were not included since, as in the case for the spinel troctolites, many of these rocks may be partial melts derived by impact melting. As such, they may not have the composition of their parent rocks and, therefore, may not convey the required information (see Addendum). Also, a number of CIPW norms for Apollo 14 rocks have been included in the data base even though these rocks probably have undergone considerable alteration. As such, these data are used with caution. However, these rocks, because they are the only ones which definitely came from great depths in the crust, are useful in this study and their general trends do follow expected patterns, even though the scatter of their points is often large.

Fourth, in addition to the pyrolite I and III compositions discussed in papers I and II, a third pyrolite (designated by the letter M) has been defined as a 50–50 mixture of pyrolite I and III for the purposes of this study. This hybrid pyrolite

was so defined because the seismic discontinuity observed at a depth of 300 km (Nakamura *et al.*, 1974; Weinrebe *et al.*, 1975) lies at a somewhat deeper and somewhat shallower depth than is predicted by the pyrolite I and III models, respectively. As is seen in Table II, which gives the pertinent data for all three pyrolite models used in this study, the upper mantle-lower mantle interface of the pyrolite M model with an Mg′ = 75 upper mantle lies at the same depth as the seismically observed discontinuity.

TABLE II

Pyrolite Moon models used in this study

Pyrolite type	III		M		I	
Mean comp.[a] of plag. in crust[b]	$Or_{0.9}Ab_{5.2}An_{93.9}$		$Or_{1.1}Ab_{4.9}An_{94.0}$		$Or_{1.3}Ab_{4.8}An_{93.9}$	
100 Mg/(Mg + Fe) of u. mantle	75	80	75	80	75	80
100 Ol/(Ol + Py) of u. mantle	9.1	26.4	19.8	36.5	32.6	48.4
Depth to u. mantle-l. mantle interface (km)	335	409	305	377	277	345
% of Moon's mass in l. mantle	53	45	56	48	59	51

[a] 20% retention model adopted in this paper
[b] The crust has a mean thickness of 61 km (Kaula *et al.*, 1974)

Fifth, according to Kaula *et al.* (1974) the mean thickness of the lunar crust is about 60 km. Thus, the scales on Figures 13, 15a and 15b in Paper II are revised. This is a minor point since the scales are only approximate in any case.

Sixth, it is assumed that, with the exception of those rocks whose compositions are clearly different from those of their parental rocks, the majority of the upland rocks have compositions which are statistically representative of the original suite of upland rocks. However, Warner *et al.* (1974) have argued that impact-induced fractionation has played a major role in the evolution of the upland rocks. If their model is correct, then the available samples most probably do not carry the information needed to define the properties of the primitive upland rocks. However, Grieve *et al.* (1974), Taylor (1975), Wood (1975b) and others have provided convincing arguments which indicate that the majority of upland rocks do have essentially the same composition as their parental rocks. Hence, it appears that the basic premise of the crustal development scheme as presented in Paper II is correct.

In addition, it has been noted that there is a drafting error in Figure 15b of Paper II. The lines connecting rocks with equal mafic contents should be straight and not slightly curved as drawn (see Figure 2 of this paper). This drafting error does not effect the boundary curves in the figure and hence none of the conclusions derived from it or from Figure 15c which utilizes only these boundary curves.

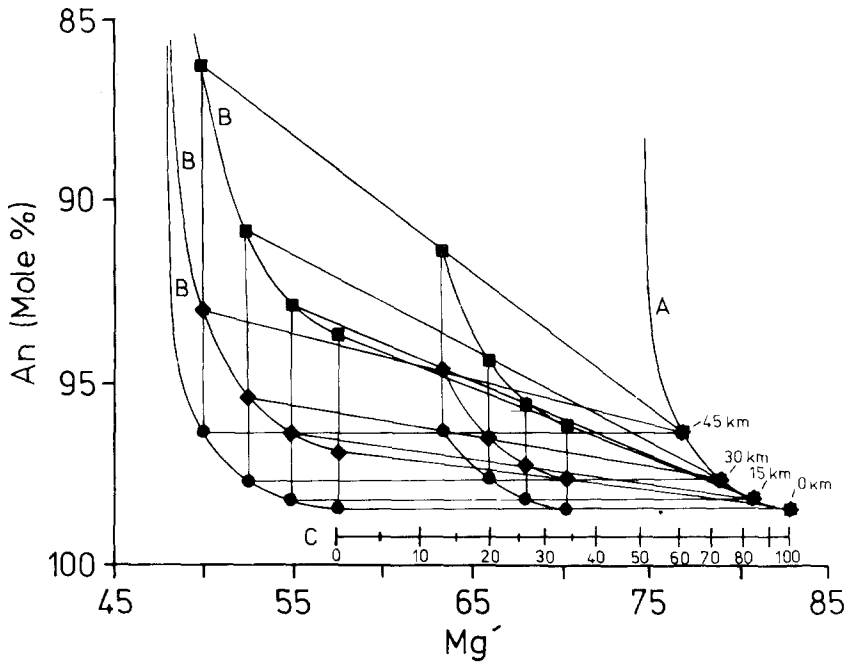

Fig. 2. Model for determining the An contents of the plagioclase vs Mg′ contents of lunar rocks formed during the development of the primitive upland crust. The model presented is based on the 20% retention, Mg′ = 75 upper mantle pyrolite M model of the Moon. Curves (A) and (B) give An vs Mg′ for rocks which were formed from plagioclase crystals plus mafic crystals and for rocks formed from plagioclase crystals plus melt, respectively. The scale labeled C gives the normalized ratio of the mafic crystals to mafic crystals plus melt which were carried along by the plagioclase crystals to form the rock. The curves marked with filled circles give the compositional data for rocks containing essentially no mafics; the curves marked with filled diamonds give the compositional data for rocks containing 25% mafics and the curves marked with filled squares give the compositional data for rocks containing 50% mafics. Families of curves are given for rocks formed when the crust was 0, 15, 30 and 45 km thick.

3. Description of the Crustal Developmental Model

Figure 2 gives a graphical representation of the analytical model developed for a moon of pyrolite M composition with Mg′ = 75 for the upper mantle (see Figures 15b and 15c and Section 5 of Paper II for the logic and data used to develop this type of model). The uncertainty in the positions of the curves in Figure 2 is about ± 1 unit of Mg′ and ± 0.3 units of An. The family of curves for each of the other pyrolite models under consideration are essentially identical to the one given in Figure 2, except that the entire set of curves is shifted to the right or left depending on the pyrolite composition and the Mg′ of the model's upper mantle. This is illustrated in Figure 3 which gives the boundary curves for the six models under consideration. As can be seen in Figure 3, there is little to distinguish between the pyrolite I, M and III models for a given upper mantle Mg′ value. However, the differences between the groups of models with upper mantle Mg′ values of 75 and 80 are great enough so that it should be possible to determine which of these two families of models is the correct one, given sufficient rock data.

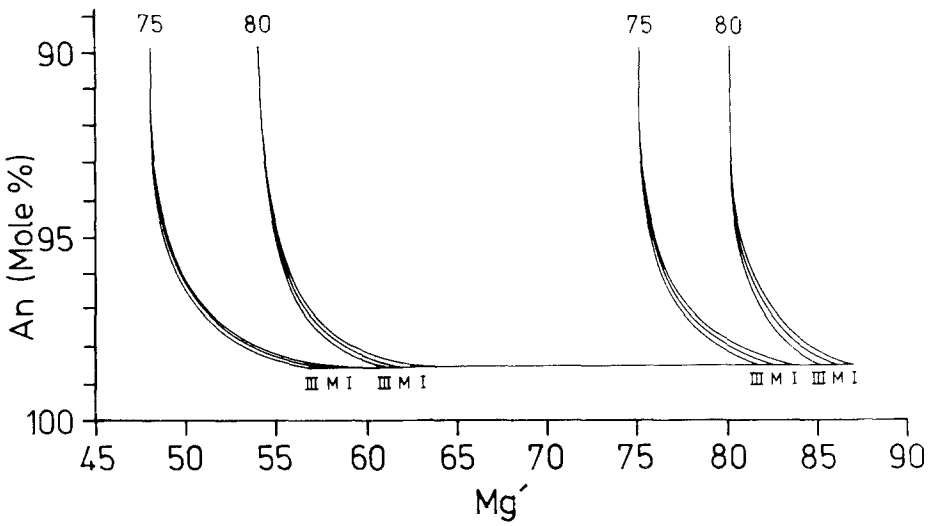

Fig. 3. Boundary curves for models of the type given in Fig. 2 for pyrolite I, M and III lunar models with upper mantle Mg′ ratios of 75 and 80.

Figure 4 gives the An contents and Mg′ values of the some 100 rocks in the data base as well as the boundary curves for the pyrolite M model with an Mg′ = 75 upper mantle. By comparing Figure 4 with Figure 3, it is clear that the Mg′ = 75 models fit the data much better than the Mg′ = 80 models do, a point which will be discussed shortly. First there are several points to be stressed regarding the fit of the data to the model given in Figure 4. Most of these points are made in Section 5 of Paper II regarding the accuracy of the proposed model in explaining the upland rock compositions. However, there are over two and a half as many data points plotted in Figure 4 as in Figure 15c of Paper II and as such, the accuracy of the model can be much better assessed. (1) With the exception of a few of the ferroan anorthosites (Dowty *et al.*, 1974b) and one Apollo 14 rock (see Paper II and the Addendum to this paper), all of the rock points lie within or near* the boundaries of the model; (2) the points at the high Mg′ end of the plot closely follow the limiting curve A which gives the composition of those rocks formed without any trapped melt; (3) the anorthosites plot along the high An boundary as expected if they formed at the beginning of the sequence; (4) the Apollo 14 rocks, though their scatter is large, plot at low An values as expected if they came from depth; (5) there is a concentration of points running from about An_{98}, Mg′ = 55 to about An_{93}, Mg′ = 74, i.e. the reversed differentiation trend predicted by the model (Paper II) and observed earlier by Steele and Smith (1973); (6) quartz normative rocks (mainly anorthosites) are found at the low Mg′ end of the plot as predicted and (7) the mean curve through the points approaches curve A at Mg′ = 75. This is expected since those rocks formed late in the sequence, when the amount of

* The uncertainty in the Mg′ and An values of the rocks, as determined when two or more sets of data are available for the same rock, are about ±1.5 and ±0.4 units, respectively. Thus, with the exceptions of the above mentioned rocks, all the rocks lie, within their errors, within the model's boundaries.

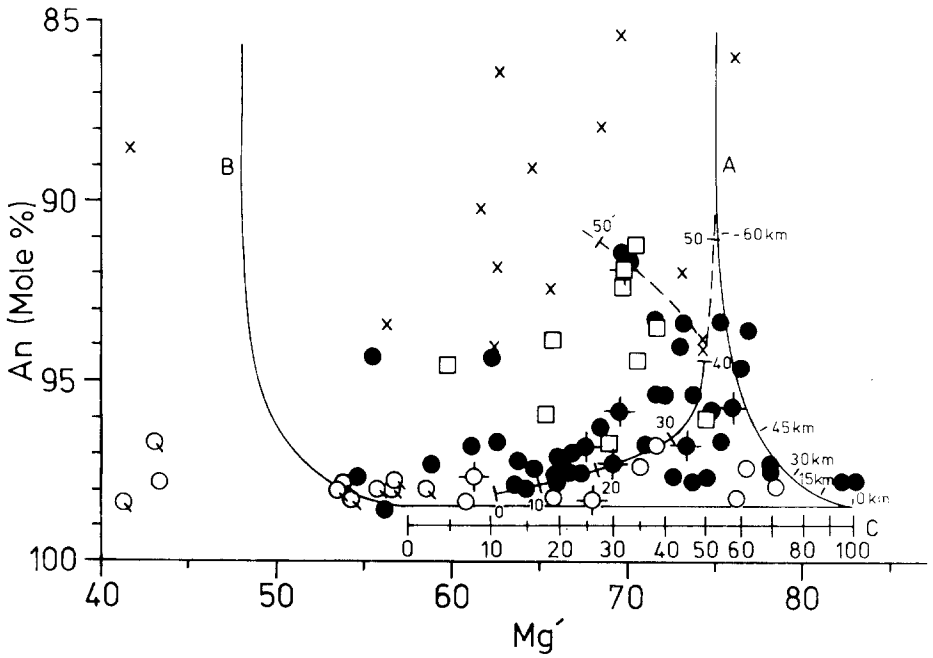

Fig. 4. An contents of the plagioclase vs Mg′ contents of the rocks in the data base. The open circles are anorthosites; the open squares are poikilitic rocks; the small x's are Apollo 14 rocks and the filled circles are all other upland rocks. The rock symbols with small tails on their lower right side are quartz normative. The rock symbols with four small radial lines are averages of sorted soil fragments. The boundaries are those for the pyrolite M model shown in Figures 2 and 3.
There are two anorthosites which plot too far to the left to be included in this diagram. These points plot at $An_{97.9}$, Mg′ = 24 and $An_{97.8}$, Mg′ = 35. See text for further discussions of the Figure.

melt was small and the olivine and pyroxene crystals in the magma were approaching their equilibrium Mg′ value of 75, must lie along curve A. However, as can be seen in Figure 4 there may be a reversal of the differentiation trend at the very end of the sequence. There are not enough data points in this part of the figure to determine if the mean curve does turn to the left at An_{94}, Mg′ = 74 or if it is asymptotic to curve A at lower An values, as such both possibilities will be considered throughout the rest of the paper. If the mean curve does turn to the left at An_{94}, this would indicate that at the end of the sequence, when convection in the region now occupied by the peridotite upper mantle (see Section 4 of Paper II) finally stopped, a small amount of melt and crystals was left at the bottom of the crust (at the KREEP zone). This magma either solidified without further differentiation or, because the system was stagnant, differentiated along the normal trend of decreasing An content with decreasing Mg′.

An additional, sensitive test of the proposed model can also be made as follows: the analytical model predicts not only the properties of the rocks discussed above, but also the upper limits of the An contents of rocks with a given mafic content and Mg′ value. These limits are shown in Figure 5 with the appropriately subdivided rock data. From this figure it is clear that, essentially all the rock points lie

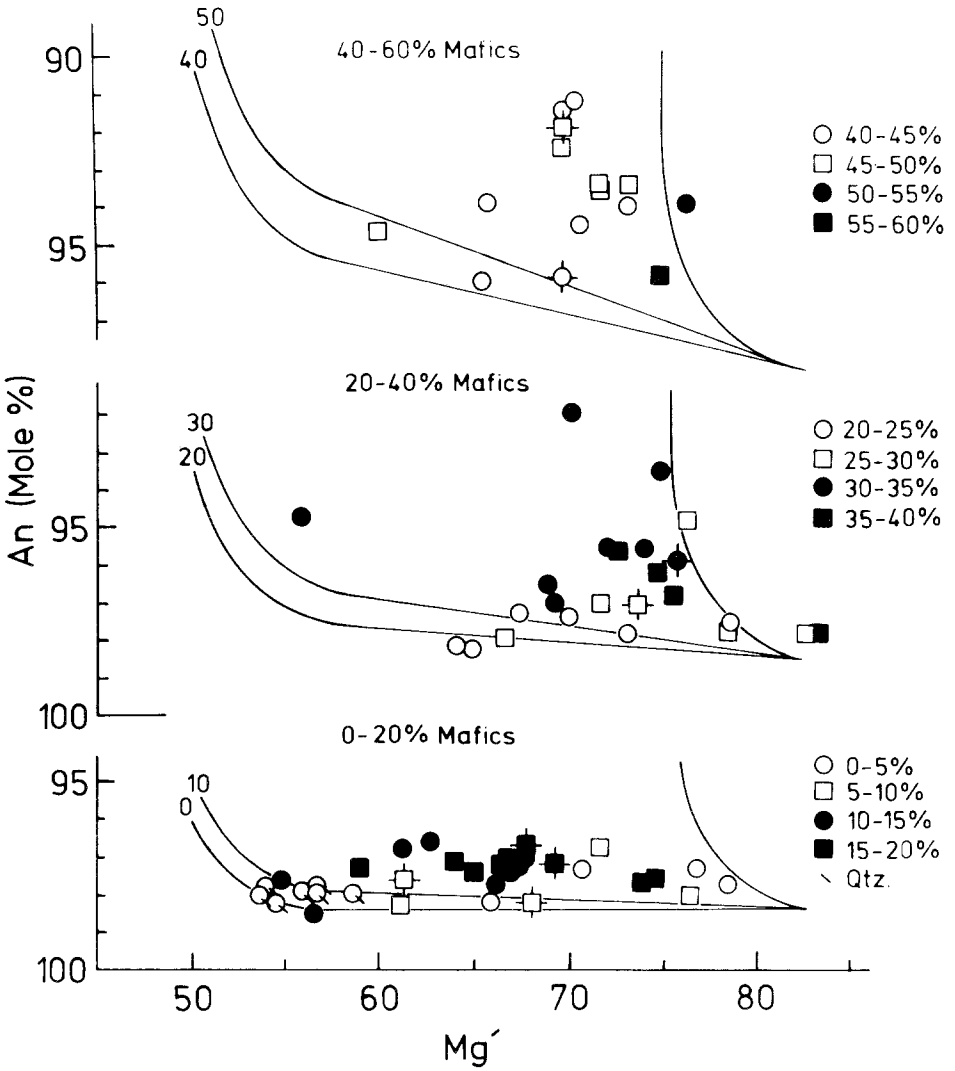

Fig. 5. An contents of the plagioclase vs the Mg′ contents of the upland rocks as a function of their mafic content. The boundaries for each set of rocks defined by their mafic content are derived from the model given in Figure 2. The rock points are the same as those shown in Figure 4 with the exception that the anorthosites at Mg′ < 45 and the Apollo 14 rocks, which most probably have been strongly modified by secondary processes, have been left off of the diagrams. Even so, the reader can see by comparing Figure 4 with this Figure that the Apollo 14 rocks, whose mafic contents range from 30–60%, lie above the 50% limiting curve, despite their large scatter.

above the limits in accordance with the model. Also, if it is not already clear from Figure 4, the data, separated in this way, show that there is a well developed trend in which the early formed high An rocks (anorthosites) are on the low Mg′ side of the plot, and the later formed rocks (high mafic content) are on the high Mg′ side of the plot, i.e. the reversed differentiation trend.

Finally, the An vs percent crystallization curve used to determine the An contents of the upland rocks in the model (i.e. curve 20 of Figure 13 in Paper II) can be calibrated in terms of the mafic contents of the resulting rocks by using the mean curve for the An contents vs mafic contents of the rocks given in Figure 6.

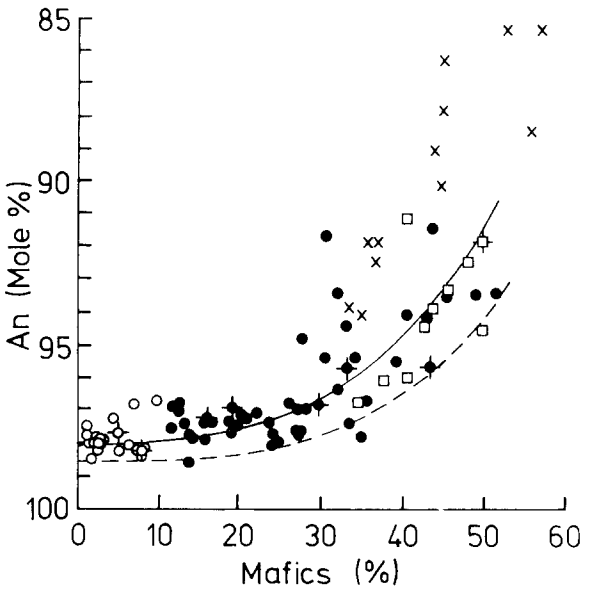

Fig. 6. An contents of the plagioclase vs the mafic contents of the upland rocks shown in Figure 4. The symbols for the various rock types are the same as in Figure 4. See the text for further discussion of the Figure.

The results of this procedure are half theoretical and half empirical, but they do lead to an interesting test of the proposed model. By integrating under curve 20, after it is calibrated in this way, one obtains the percent of rocks formed as a function of their mafic contents, see Figure 7. The results indicate that the most abundant rocks in the crust should contain about 32% mafics and that on average the rocks contain about 28% mafics. Further, anothosites and mafic rich rocks (~50% mafics) should be relatively rare. These results are in agreement with observations (e.g., as reviewed by Taylor, 1975) that the average and the most abundant rock type of the lunar crust is anorthositic norite with 70% plagioclase, 20% orthopyroxene, 9% olivine and 1% ilmenite and that anorthosites and other rock types are much less abundant in the upland crust than the anorthositic norites.

Thus, it appears that the additional data tend to confirm the conclusions drawn in Paper II regarding the validity of the proposed model for explaining the compositional variations of and formation of the primitive suit of upland rocks. As mentioned above, the data also show that models with Mg′ = 80 are most probably not valid. It is therefore concluded that the correct equilibrium value of Mg′ for the magma system from which the crust and upper mantle formed is about 75 and hence this is the Mg′ value of the peridotite upper mantle. Assuming that the

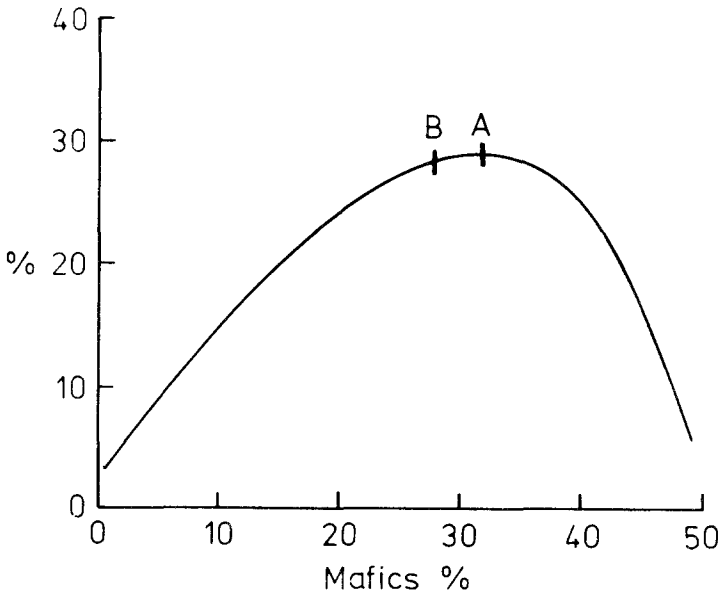

Fig. 7. Percent of rocks formed vs their mafic content. The most frequent rock type contains about 32% mafics (point A) and the average mafic content of the upland rocks is about 28% (point B).

proposed developmental sequence is correct, this determination of the Mg′ value of the upper mantle is as sensitive, if not more so, as the determinations of this quantity made by Ringwood and his associates (e.g., Ringwood and Essene, 1970; Green and Ringwood, 1972, 1973; Ringwood, 1975) and others from experimental work done on mare basalts. However, this is a moot point since the results obtained by these two methods are in agreement; a review of the published results indicates that the majority of the mare basalt samples studied crystallized from magmas whose source areas have Mg′ = 75. Only rarely do the experimental data indicate that the source area of the magma of a sample has a different value of Mg′ (e.g. Mg′ = 80 for rock 12040, Green *et al.*, 1971). However, such small variations from the mean value are well within the expected range of compositional variations in the upper mantle (see Section 4 of Paper II).

4. Information Derived from the Crustal Model

If the model shown in Figure 4 is accepted as the best fit to the lunar rock data, then one can proceed to derive the mean amounts of plagioclase, pyroxene and olivine crystals and trapped melt which together made up the various upland rocks as the crust grew in thickness. The curve drawn through the points in Figure 4 gives the mean Mg′ of the rocks as a function of their An contents and hence as a function of crustal thickness (see Figure 13 of Paper II). This curve is calibrated in terms of the mafic contents of the rocks by using the curve in Figure 6. The nonlinear scale immediately below the lower An boundary curve in Figure 4 gives the

normalized ratio (C) of the mafic (olivine and pyroxene) crystals (T_m) to mafic crystals plus melt (T_1), (i.e. $C = 100\ T_m/(T_m + T_1)$) trapped by the cumulating plagioclase crystals. This scale is strictly valid only for $An_{98.5}$. To be valid for other values of An, it has to be stretched or compressed and shifted to the left or right so that zero and 100 are always on the B and A curves, respectively, at the desired value of An.

The nonlinearity of the C scale is due to the fact that the peritectic melt trapped by the plagioclase crystals solidifies (approximately) to 50% plagioclase and 50% pyroxene (see Section 5 of Paper II). As is obvious, the trapped mafic crystals (whose Mg′ is determined from curve A) and the pyroxene (P) crystallized from the trapped melt (whose Mg′ is determined from curve B) mix together to yield mafics with an intermediate value of Mg′. This Mg′ value varies linearly with the mixing ratio (Δ) where Δ is $100\ T_m/(T_m + P)$. Since only 1/2 of the trapped melt crystallizes to pyroxene, $T_1 = 2P$ and so C can be written as

$$C = 100\ T_m/(T_m + 2P), \tag{1}$$

from which it can be seen that

$$C \propto (T_m + P)/(T_m + 2P); \tag{2}$$

and, hence, that C varies nonlinearly with Mg′.

As is deduced from Figure 15a of Paper II and from Figures 2 and 5 of this paper, the An content of the plagioclase of a rock formed at any point in time in the sequence is related to, but generally less than the An content of the plagioclase crystallizing from the melt at that time. This is due to the trapping of melt which lowers the final An value of the feldspars of the rock. However, the scale discussed above gives C for the rock only when the scale is placed on the diagram at the An value the plagioclase had before the forming rock trapped the melt. Thus the scale will be below the rock point to be measured (except for rocks along curve A which contain no trapped melt and, therefore, for which the scale is superfluous). This value of An is not known initially but must be found before C can be determined. There are two ways of estimating limiting values of An. First, if it is assumed that the rock trapped virtually no melt, the scale is shifted to coincide with the point and the maximum value for C can be determined. The minimum value for C can be found using the data given in Figure 6. While the best fit curve through the points gives the mean An vs mafic contents of the rocks, the lower envelope curve (dashed curve) gives the maximum An contents of the rocks of a given mafic content. The An value derived from the envelope curve corresponds to the An contents of the plagioclase crystallizing directly from the melt, i.e. the value needed, assuming no scatter in the data. However, the scatter prevents An_{max} from being uniquely determined. Even so, the envelope curve does give an upper limit for An_{max} and this value can be used to set the scale on the A and B curves in order to obtain the lower limit of C for the rock point in question.

Using the above described procedures, C_{max} and C_{min} can be determined for any rock point. From these C's one can derive the amounts of trapped melt (T_1), trapped mafics (T_m) and original plagioclase (C_p) as follows: The amount of pyroxene (P)

which crystallized from the trapped melt is $T_1/2$, thus the total amount of mafic minerals (M) in the rock is given by

$$M = T_m + T_1/2. \tag{3}$$

By definition,

$$\frac{C}{100} = T_m/(T_m + T_1) = C'; \tag{4}$$

thus Equations (3) and (4) yield

$$T_1 = 2M(1 - C')/(1 + C'). \tag{5}$$

Since T_m is known for all rocks, the computed value of T_1 obtained from Equation (5) together with Equation (3) give

$$T_m = M - T_1/2 \tag{6}$$

and, similarly,

$$C_p = 1 - M - T_1/2. \tag{7}$$

The derived quantities C_p and $T_1/2$, the observed An content of the rock (An_r) and the empirical data giving the An contents of crystals (An_c) vs the An contents of the melt (An_m), as derived from the albite-anorthite phase diagram, can be used to compute the An contents of C_p since

$$An_r(C_p + T_1/2) = An_c C_p + An_m T_1/2. \tag{8}$$

The values thus obtained for C_{max} and C_{min} bracket the correct value of C and, of course, the values of An derived from these values of C bracket the correct value of An. Using these maximum and minimum values of An as second estimates as to where on curves A and B the C scale should be set, the procedure can be repeated until, by iteration, the derived values of C and An converge on the real values. In practice, the correct values of C, T_1 and An can readily be estimated based on the results obtained from the first estimates of An_{max} and An_{min}.

TABLE IIIA

Estimates of the initial components of the primitive upland rocks

Mafic content (%)	Estimates of C (%)		Trapped melt (T_1) (%) based on		An contents of C_p based on	
	C_{min}	C_{max}	C_{min}	C_{max}	C_{min}	C_{max}
2	12	21	3.1	2.6	98.2	98.2
10	18	30	13.9	10.8	98.2	98.2
20	34	45	19.7	15.2	98.1	98.0
30	62	72	14.1	9.9	97.3	97.1
40	81	92	8.4	3.5	95.0	94.5
[a]50	94	97	3.1	1.5	91.6	91.3
[a]50′	58	61	26.6	24.3	94.7	94.5

[a] Values derived from the two possible branches of the mean curve in Figure 4.

TABLE IIIB

Initial components of the suite of primitive upland rocks

Mafic content (%)	Trapped melt (T_1) (%)	Trapped mafics (T_m) (%)	Original plagioclase (C_p) (%)
2	3	0.5	96.5
10	12	4.0	84.0
20	18	11.0	71.0
30	13	23.5	63.5
40	5	37.5	57.5
[a]50	2	49.0	49.0
[a]50′	26	37.0	37.0

[a] Values derived from the two possible branches of the mean curve in Figure 4.

The results obtained by these procedures for a number of points along the mean curve in Figure 4 are given in Tables IIIA and IIIB. Also, Figure 8 gives the maximum, minimum and final values for T_1 for the mean rock curve in Figure 4. The values given in Tables IIIA and IIIB and in Figure 8 are strictly correct only for the pyrolite M model. However, the differences between these values and those obtained for the pyrolite I and III models are negligible and so the data given will be used for all three models in the following discussions.

5. Variations in the Olivine, Pyroxene and Quartz Contents of the Upland Rocks and their Implications for the Differentiation Sequence

Using the data given in Tables IIIA and IIIB and Figure 8 and information derived from the proposed crystallization sequence, it is possible to compute the expected olivine to olivine plus pyroxene ratios (Ol′), normalized to 100, or the quartz to quartz plus pyroxene ratios (Qtz′), normalized to 100, of the rocks based on the models and to compare these values with those obtained from the CIPW norms of the data base rocks.

Figure 9 gives the previously proposed (Papers I and II) crystallization paths for the three pyrolite models still under consideration. Using model M as an example and using the lunar mass (L_m) as a mass unit, the point where the isolation of the early olivine in the lower mantle stopped and equilibrium crystallization began (as indicated by the x) occurred when 0.59 L_m had crystallized. The Alkemade line was crossed when 0.65 L_m had solidified. Thus, some 0.06 L_m mass remained olivine throughout the rest of the sequence and remained mixed with the melt. The olivine-pyroxene cotectic was reached when 0.70 L_m had crystallized as olivine; however, 0.05 L_m of olivine, i.e. the amount which formed between the Alkemade line and the cotectic, was altered to pyroxene during the remaining sequence. The olivine-pyroxene-anorthite peritectic was reached when 0.80 L_m had crystallized. As the composition of the melt moved along the cotectic to the pertectic, 0.10 L_m of pyroxene solidified and 0.02 L_m of olivine was converted to pyroxene. Finally, the peritectic crystallization yielded 0.10 L_m of pyroxene and 0.10 L_m of anorthite and 0.03 L_m of olivine was converted to pyroxene during this process. The sequences for

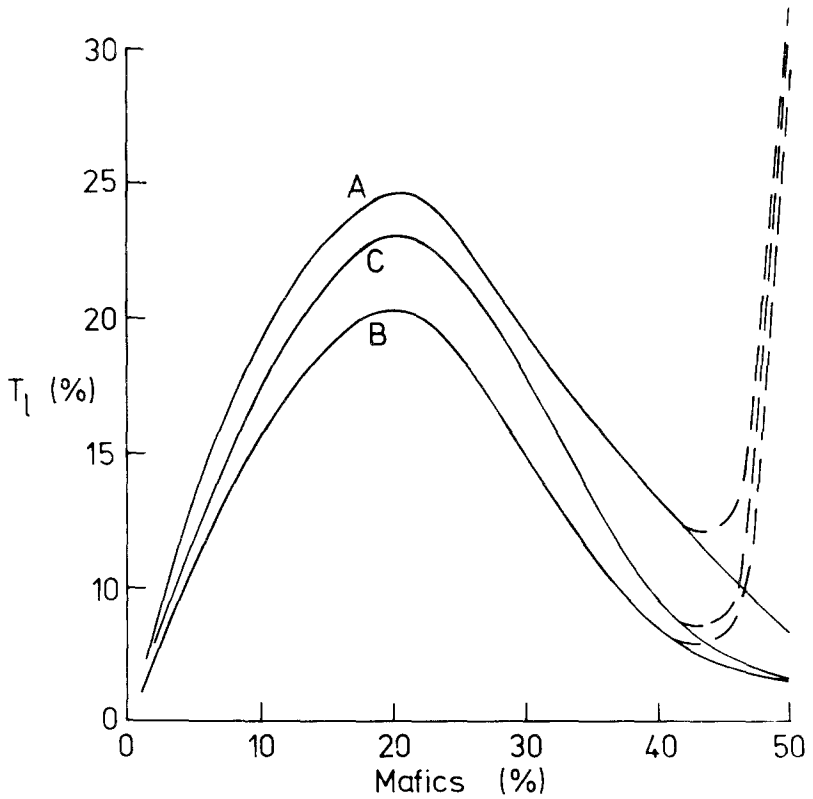

Fig. 8. Amounts of melt (T_1) trapped by the plagioclase crystals vs mafic content of the final rock. The curves given are the maximum (A), minimum (B) and final (C) values derived from the data given in Tables IIIA and IIIB. The solid and dashed branches of the curves beyond 40% mafics give the values derived for the two branches of the mean curve in Figure 4.

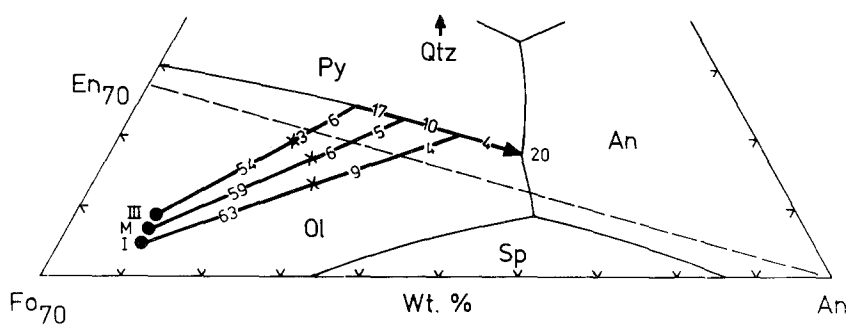

Fig. 9. Crystallization paths for Moon models based on pyrolite I, M and III compositions with upper mantle Mg′ = 75 and the peritectic sequence. The numbers along the various segments of the paths give the percent of the Moon which crystallized along that segment. The paths are plotted on a pseudo-ternary liquidus diagram for the system olivine (Fo_{70}), anorthite and silica (after Walker *et al.*, 1973).

the pyrolite I and III models are similar except, of course, the amounts of olivine, pyroxene and plagioclase formed are different as is indicated in Figure 9.

Assuming that the rate of the alteration of olivine to pyroxene was linear during the peritectic crystallization, it is possible to compute the Ol′ crystals in the magma from which the crust and upper mantle formed. The pertinent quantities, derived from Figure 9, are given in Table IV and the results are plotted in Figure 10. The calibration of the curves in Figure 10 in terms of the percent mafics in the upland

TABLE IV

Olivine and pyroxene contents of the magma during the peritectic crystallized sequence

Pyrolite model	Pyroxene content at beginning of sequence (%)[a]	Olivine changed to pyroxene during sequence (%)[a]	Olivine remaining at end of sequence (%)[a]
I	4.8	3.2	8.5
M	11.8	3.2	6.1
III	19.8	3.2	3.0

[a] % of Moon's mass

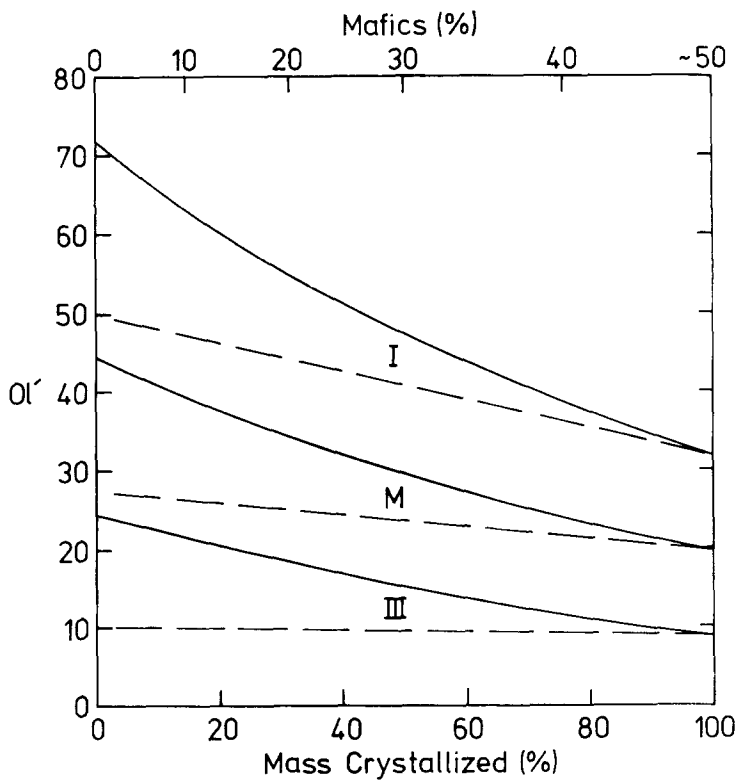

Fig. 10. Ol′ ratios of the mafic crystal in the magma during the peritectic sequence and 6% Qtz cotectic sequence (solid curves) and the 0% Qtz cotectic sequence (dashed curves). The pairs of curves are for the pyrolite I, M and III models with final Mg′ values for the upper mantle of 75.

rocks (upper scale) is accomplished via the mean mafic vs An curve in Figure 6 and curve 20 in Figure 13 of Paper II (with an adjusted depth scale as discussed above).

According to the developmental sequence described in Section 5 of Paper II and in Section 4 above, the mafics in the upland rocks consist partially of crystals (whose Ol′ is given in Figure 10) trapped from the magma and partially of those crystallized formed from the trapped melt. Using the data in Table IIIB on T_1 and T_m and the curves given in Figure 10, it is possible to calculate the amounts of trapped olivine (T_o) and pyroxene (T_p) crystals, the amount of pyroxene (P) crystallized from the trapped melt (T_1) and the amount of normative quartz (Qtz_m) in the trapped melt. Now, T_o is given by

$$T_o = T_m Ol', \tag{9}$$

where Ol′ is the value for the trapped mafics as given in Figure 10. Similarly, T_p is given by

$$T_p = T_m(1 - Ol'). \tag{10}$$

As above,

$$P = T_1/2. \tag{11}$$

The amount of normative quartz in the peritectic melt is ~6%, leading to

$$Qtz_m = 0.06T_1. \tag{12}$$

For Mg′ = 70 – i.e., the mean value for upland rocks – 2.6 weight per cent of olivine reacts with 1 weight percent quartz to make 3.6 weight percent pyroxene. Thus, when a mixture of olivine, pyroxene and quartz are trapped together and allowed to react to equilibrium, the final amounts of pyroxene (P_f) and olivine (Ol_f) or quartz (Qtz_f) are given by

$$P_f = P + T_p + 3.6Qtz_m \tag{13}$$

and

$$Ol_f = T_o - 2.6Qtz_m \tag{14}$$

for $T_o > 2.6Qtz_m$; otherwise for $2.6Qtz_m > T_o$

$$P_f = P + T_p + 1.38T_o \tag{15}$$

and

$$Qtz_f = \frac{2.6Qtz_m - T_o}{2.6}. \tag{16}$$

These quantities yield Ol′ for the final rock or Qtz′ if the rock is quartz saturated. For better comparison with Ol′, Qtz′ is defined as

$$Qtz' = \frac{100(2.6Qtz_f)}{2.6Qtz_f + P_f}, \tag{17}$$

where $2.6Qtz_f$ is the olivine equivalent of the quartz in the rock.

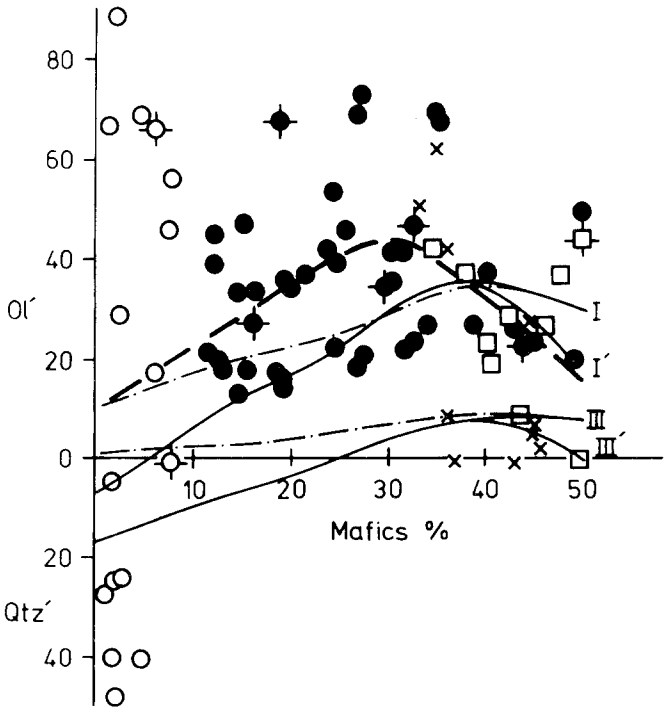

Fig. 11. Ol′ and Qtz′ of the rocks in the data base vs their mafic content. The heavy dashed curve gives the mean of the rock data. The solid curves give the computed values Ol′ for pyrolite I and III models based on the peritectic sequence and the 6% Qtz cotectic sequence discussed in the text. The dashed-dotted curves give the Ol′ values for the 0% Qtz cotectic sequence. The branches of the curves between 40 and 50% mafics correspond to the two branches of the mean curve of Figure 4. The rock symbols are the same as those in Figure 4.

The quantities Ol′ and Qtz′ so derived are given in Figure 11 for pyrolite models I and III as well as Ol′ and Qtz′ for the rocks in the data base. Due to the large scatter in the rock data, a mean curve (heavy dashed line) through the points is given for reference. From Figure 11 it is clear that the models fail to give the correct Ol′ values as a function of mafic content of the rocks. It is true that, as discussed in Section 5 of Paper II, the trend towards quartz normative rocks at low mafic contents is correctly modeled and the general shape of the curves is correct. However, both curves (the curve for pyrolite M lies between the curves for pyrolite I and III) lie well below the mean curve in the figure. These results clearly indicate that the upland rocks are much richer in olivine than the models developed in Papers I and II predict. This could mean that the terrestrial mantle and, hence, the Moon is richer in olivine than is indicated by even the pyrolite I composition. However, this seems very unlikely and since the pyrolite models developed match all other lunar properties quite well, it is much more likely that the problem lies elsewhere.

Now, the basic, simplified assumptions behind the differentiation sequence adopted in Paper I and retained in Paper II are that the crystallization occurred at the surface (and later at the under side of the forming crust) and that the early formed

olivine crystals and the later formed pyroxene crystals sank to form the lower and upper mantles, respectively. While this sequence is reasonable, it apparently does not fully explain the lunar sequence as indicated by the failure of the Ol′ values computed for the crustal rocks to match the observed values. Recently Walker *et al.* (1975) have discussed the probable crystallization sequence in a "very thick magma body". As they point out, the experimental data are still insufficient to determine exactly what happens in such a system and the predicted effects depend critically on a number of factors – e.g., melt composition, temperature gradients, compositional gradients, rates of crystal settling, effects of convection, etc. However, for such a system it seems probable that as olivine, which crystallizes near the surface (at low pressure), sinks in a liquid that is saturated or nearly saturated with pyroxene or plagioclase, it will react with the liquid at depth and be converted to pyroxene. This is due to the fact that, for such a liquid, olivine is the liquid phase at low pressure but pyroxene is the liquid phase at pressures greater than a few kilobars. Hence, the sinking olivine eventually reached a depth where it is unstable and reacts to form the stable phase – pyroxene.

Now, in the case of a pyrolite Moon, the liquid is saturated with olivine for about the first half of the crystallization sequence (see Figure 11 of Paper II or Figure 9 of this paper). Thus, as discussed in Papers I and II, the early high Mg′ olivine crystallized out at the surface and sank through the melt, which has olivine as the liquid phase at all pressures of interest, to form the lower mantle. However, as the composition of the melt approached the olivine-pyroxene cotectic (see Figure 9), i.e. as the melt neared saturation with pyroxene, the conditions at depth became such as to cause the sinking olivine to react with the melt to form pyroxene. According to Walker *et al.* (1975) it is also possible for some pyroxene to crystallize directly from the melt at depth under these conditions. When this process(es) began, the lower mantle formation sequence ended and the upper mantle development began.

As is required in order to have a nearly uniform upper mantle (see Section 5 of Paper I and Section 4 of Paper II) and as is a consequence of the conversion of olivine to pyroxene at depth (see below), the magma above the early formed dunite lower mantle was well stirred by convection. Hence, as olivine continued to crystallize and at least partially be converted to pyroxene at depth, the composition of the melt stopped moving radially from the olivine corner of the phase diagram and began to move off towards the right from the point where the reaction at depth started, see Figure 12. The exact path is determined by the percent of olivine which was being converted to pyroxene, a quantity which was most probably variable during the sequence. However, for simplicity it is assumed that the conversion rate was constant and for a reasonable range of resulting Ol′ for the mixture ($45 > Ol' > 25$ for pyrolite M as shown in Figure 12) the crystallization path intercepted the olivine-anorthite cotectic when 80% of the Moon had solidified. At Ol′ values higher than about 45, the crystallization path intersects the olivine-pyroxene cotectic and the crystallization sequence is essentially identical to the one originally proposed (hereafter referred to as the peritectic sequence); thus, there is no change in the derived Ol′ values. Therefore, the new sequence (hereafter referred to as the cotectic sequence) is of interest only in those cases where the crystallization

path intersected the olivine-anorthite cotectic. Now, at the point where plagioclase began to co-crystallize with olivine, the majority of the plagioclase floated up to begin the formation of the crust and the majority of the olivine sank into the convecting mass of melt, pyroxene crystals and olivine crystals which later became the upper mantle.

Thus, the cotectic sequence is similar to the old peritectic sequence, except that there are two significant changes in the chemical system present when the crust was forming in the cotectic sequence as compared to the peritectic sequence. First, the amount of normative quartz in the melt was anywhere from 0% to 6% depending on where the cotectic was intersected and how far down the cotectic the composition of the melt moved during the final crystallization of the Moon. Second, olivine and plagioclase were co-crystallizing and not pyroxene and plagioclase. The effects of the reduced amount of normative quartz in the melt on the Ol′ of the final rocks can be seen in Figure 11 which also gives the Ol′ values computed for the limiting cotectic case where $Qtz_m = 0$ (see details below). As can be seen, this effect alone brings the theoretical curves for the pyrolite I model into better accordance with the observational data, though the pyrolite M and III model curves are still too low. However, it is unreasonable to assume that the cotectic melt was not saturated in quartz. If this were the case, it would not be possible to account for the early quartz normative anorthosites (see Figure 4 and the discussion given in Section 5 of Paper II on the quartz normative rocks). Thus, unless all the quartz normative rocks have secondary origins (for which there is some evidence (Wood, 1975b)), it is necessary and reasonable to assume that the crystallization path of the Moon intersected the cotectic on the quartz side of the Alkemade line, see Figure 12.

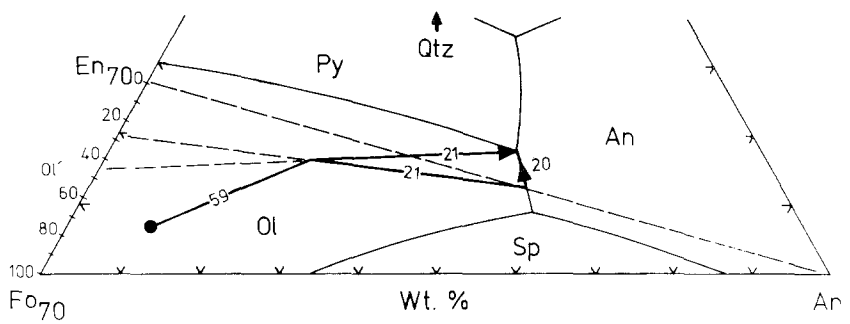

Fig. 12. Crystallization path of the pyrolite M model with upper mantle Mg′ = 75 for the cotectic sequence. The intersections of the dashed lines, emanating from the point in the olivine volume where the path moves off to the right, with the Ol′ scale on the left side of the diagram indicate the Mg′ ratio of the mafics in the magma during that part of the sequence. The numbers along the various segments of the paths give the percent of the Moon which crystallized along that segment. The paths are plotted on a pseudo-ternary liquidus diagram for the system olivine (Fo_{70}), anorthite and silica (after Walker *et al.*, 1973).

This requirement ensures that early rocks with very low values of C are quartz normative, as observed. This restriction and the one discussed above that the crystallization path must intersect the olivine-plagioclase cotectic indicate that, for the pyrolite M model (as given in Figure 12) the Ol′ of the mafic crystals in the

melt at the time when the cotectic crystallization began was between 27 and 45. The upper limit is, of course, the same as the value of 45 derived for Ol′ at the beginning of the formation of the crust in the peritectic sequence.

Table V gives the Ol′ values of the mafics and the amount of normative quartz in the melt at the beginning and end of the sequence and the percent of the Moon crystallized for all three models for both the peritectic and the cotectic sequence. As can be seen from Table V, there is no difference between the peritectic

TABLE V

Compositional and physical properties of the crust – upper mantle magma system

Pyrolite model	Peritectic sequence					Cotectic sequence				
	beginning		end		% of Moon crystallized	beginning		end		% of Moon crystallized
	Mg′,	Qtz_m	Mg′,	Qtz_m		Mg′,	Qtz_m	Mg′,	Qtz_m	
I	72	6%	32	6%	20	[a]50	0%	[a]32	0%	20
						72	6%	32	6%	
M	44	6%	20	6%	20	[a]27	0%	[a]20	0%	20
						44	6%	20	6%	
III	26	6%	9	6%	20	[a]10	0%	[a] 9	0%	20
						26	6%	9	6%	

[a] Upper and lower sets of values are for the models where the cotectic line is intersected at Alkemade line (hence 0% Qtz) and very near the olivine-pyroxene-plagioclase peritectic (hence 6% Qtz), respectively (See Figure 12).

sequence and limiting (6% Qtz_m) cotectic sequence in terms of the quantities presented. Thus, the changes in Ol′ with advancing crystallization are the same for both sequences and the curves given in Figure 10 can also be used for the limiting (6% Qtz_m) cotectic model. However, as can be seen in Figure 10 (dashed curves) and Table V, the Ol′ for the 0% Qtz_m limiting case for the cotectic sequence is always (except at the end of the sequence) lower than for the 6% Qtz_m case. Taking this effect into account and the lack of quartz in the melt, one derives the second set of curves in Figure 11. The reader can interpolate (linearly) between the limiting curves in Figure 11 for 0% and 6% quartz and see that curves for 1 to 3% quartz yield model curves for all three pyrolite models which are still lower than the observational means, though the pyrolite I model is not too low. However, it is still clear that the Ol′ of the trapped mafics is too low in order to account for the observed data.

Now, the second property of the cotectic crystallization scheme, i.e. that olivine and plagioclase were co-crystallizing, comes into play in the development of the crustal rocks. It seems most likely that, as the plagioclase crystallized out, it will have had a tendency to trap co-crystallizing olivine as well as trapping olivine and pyroxene from the circulating mass of mafic crystals and melt immediately below the growing crust. Since this is most probably the case, the amount of trapped olivine is much greater than is indicated by the curves in Figure 10 and hence the Ol′ of the resulting rocks would be much higher than is indicated above. The reverse is also probably true for the peritectic case since the co-crystallizing pyroxene would

have been preferentially trapped by the plagioclase, thereby lowering the already too low Ol′ computed for the rocks using the peritectic model.

There are a number of possible combinations for the ratio of trapped co-crystallizing olivine to mafics trapped from the circulating magma. However, as is shown in Figure 13 (curve a–a′) for the pyrolite M model, if the mixing ratio between

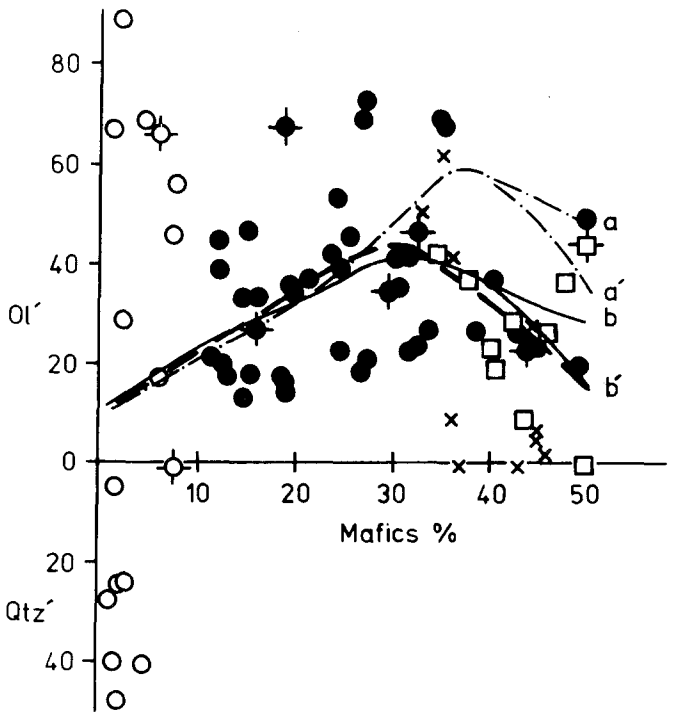

Fig. 13. Ol′ and Qtz′ of the rocks in the data base vs their mafic content. The heavy dashed curve gives the mean of the rock data. The theoretical curves are for a pyrolite M model and a cotectic sequence. Curve a–a′ gives the computed Ol′ values for the case where co-crystallizing olivine is trapped along with circulating mafics by the plagioclase. Curve b–b′ is similar to a–a′, but takes into account the effect of the probable co-crystallization of pyroxene towards the end of the sequence. See text for full explanation of the logic for these curves.

co-crystallizing olivine and trapped mafics is held constant at 1 to 1 while the quantity of normative quartz in the melt increases from 1% to 6% (as the melt composition moves along the cotectic towards the peritectic), the computed Ol′ values are initially correct, but are too high at the end of the sequence. However, as the melt composition approached the peritectic, pyroxene most probably began to co-crystallize with plagioclase and olivine over a small depth range below the crust. If so, this effect would reduce the Ol′ ratio of the trapped mafics towards the end of the sequence. Taking this into account then, an exact fit to the observed data for all three models can easily be obtained, see curve b–b′ of Figure 13. Thus, the variations in Ol′ of the primitive upland rocks can readily be accounted for if the cotectic sequence is correct.

Unfortunately, there is a lack of a unique set of conditions required to match the rock data. This is the case since the mixing ratio of the trapped co-crystallizing mafics to the trapped circulation mafics and the amount of normative quartz in the trapped melt at any point in the sequence are all governed by a wide set of conditions, e.g. the compositional balance between the melt and the crystallizing and reacting phases, the point on the cotectic where the co-crystallization began, the depth at which olivine was being converted to pyroxene, the rate of convective turnover, etc. Thus, this lack of uniqueness prevents one from being able to determine which of the model pyrolite compositions best matches the composition of the Moon.

The information required to distinguish between these three models is by and large seismic and experimental petrology data. At present the uncertainty in the depth of the 300 km discontinuity is at least 30 km (Nakamura *et al.*, 1974; Weinrebe *et al.*, 1976) and it is of course not known whether the depth of the discontinuity now measured in the vicinity of the Apollo seismic stations (mainly near Apollo 12 and 14 stations) is representative of the entire Moon or not. When the depth of the discontinuity is better known and when better seismic profiles for the upper mantle and the upper part of the lower mantle are available, the models can be critically tested. To date it is only possible to conclude that the existence of the discontinuity at 300 ± 30 km is in accordance with the prediction of a compositional discontinuity (and hence a velocity discontinuity) between 277 and 335 km, see the models in Table II with $Mg' = 75$.

The experimental petrology data by Ringwood and his associates (e.g., Ringwood and Essene, 1970; Green *et al.*, 1971; Green and Ringwood, 1972, 1973) and others which lead to the identification of a pyroxenite or peridotite source material for the mare basalt magmas can be used to indicate which models might be the more reasonable ones. The Al_2O_3 and CaO contents of the pyroxenes of the upper mantle are given in Table VI, from which it can be seen that the pyrolite III model offers the best match and the pyrolite I the poorest match to these data.

TABLE VI

Al_2O_3 and CaO contents of pyroxenes in the upper mantle according to models and experimental data

Pyrolite model	Al_2O_3 (%)	CaO (%)
I	8.2	6.5
M	5.7	6.2
III	4.1	5.8
Experimental data on mare basalts	4–5	4–5

Similarly, it is noted in Figure 9 that the point in the crystallization sequence where the early olivine stopped being isolated in the lower mantle and olivine began to be converted to pyroxene is increasingly farther from the olivine-pyroxene cotectic for the Sequence III, M and I. Thus, even though the desired experimental data are lacking, the likelihood that olivine began being converted to pyroxene at depth at

the point indicated for the pyrolite models also decreases from III to I. Hence, both of these compositional properties indicate that the pyrolite III model best represents the Moon. However, the data are not decisive and so additional data are required to answer this question.

There are a few additional points to be made regarding the cotectic sequence. First, as discussed in Papers I and II, the nearly homogeneous composition of the upper mantle indicates that it was formed as a result of equilibrium crystallization and the Mg′ balance of the entire Moon requires that the lower mantle was formed under disequilibrium conditions. However, there is no explanation, in terms of the peritectic sequence, as to why convection in the magma was weak enough so that the first 55 to 60% of the Moon could crystallize and sink undisturbed to form the dunite lower mantle. Then as pyroxene began to crystallize the convective motion became so strong that the newly formed crystals were kept suspended in the melt, where they reacted, until the crystallization of the Moon was nearly complete. However, the physics of the cotectic sequences clearly indicated not only what caused the large increase in convective activity but also why it increased at just the right time in the sequence to satisfy the compositional constraints. The answer to these questions lies in the fact that the conversion of olivine to pyroxene is an exothermic process. Thus, as soon as the composition of the melt was nearly saturated in pyroxene, the conversion process began at depth ($\sim$300 km) in the magma and as a result considerable quantities of heat were released in the lower levels of the liquid-crystal system. This would of course result in a rapid increase of the rate of convection. Hence, the compositional constraints themselves dictated when the strong convective activity began in order to form the nearly uniform upper mantle.

Second, as shown above, the cotectic model can readily account for the observed Ol′ ratios of the primitive suite of upland rocks which typically contain 20 to 40% olivine (see Figure 11 or 13). However, as has long been noted (Prinz *et al.*, 1973b), troctolites are an important member of the upland suite of rocks. While it is probable that some of the troctolites are early cumulates from impact generated melts (as is apparently the case for the spinel troctolites), it is also quite likely that many of the troctolites are early, primitive cumulates as suggested by Prinz *et al.* (1973b). As is obvious, troctolites can readily be produced during the cotectic crystallization sequence. Such rocks would have formed mainly from co-crystallizing plagioclase and olivine with little or no trapped melt. As such, the troctolites (and anorthosites with high Ol′) should have a strong tendency to plot near or along the A boundary curve in Figure 4. As is shown in Figure 14, this is the case.

Third, it is noted that, due to the convective motion in the magma system, the newly formed pyroxene crystals would be brought back to the vicinity of the surface where they would be unstable. They would then have a tendency to withdraw heat from the system and re-convert to olivine during that time in the convective cycle where they were near the surface. This process would of course be repeated and so the crystals would go through the conversion cycle many times, thus ensuring a relative homogeneous composition for the upper mantle. However, the system continually convecting magma mass, within which pyroxene was the stable phase, grew with time. Thus, the reaction ol + melt $\rightarrow$ py. would have dominated over the

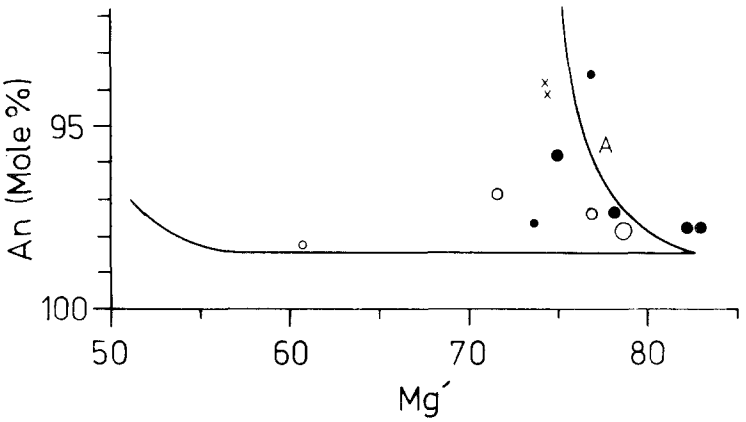

Fig. 14. An contents of the plagioclase vs Mg′ ratios of the troctolites and anorthosites in the data base with Ol′ > 50. The rock symbols are the same as in Figure 4. The smallest symbols are for rocks with 50 < Ol′ < 65; the intermediate sized symbols are for rocks with 65 < Ol′ < 80 and the largest symbols are for rocks with 80 < Ol′ < 95. The boundary curves are the same as those in Figure 4.

reverse reaction and the net effect of the convectively cycling would have been to produce pyroxene.

The final point to be made is in regard to the spinel troctolites. It has been suggested that the spinel troctolites are members of the earliest primary cumulated found on the Moon (e.g., Prinz *et al.*, 1973a, 1973b) Now, as is seen in Figure 12, if the conversion of olivine to pyroxene at depth were extremely efficient, then the crystallization path of the Moon would intersect the olivine-spinel cotectic before moving to the olivine-plagioclase cotectic. If this were the case, the spinel dunites would have formed as the melt composition moved along the olivine-spinel cotectic. Though it seems very unlikely, since the magma was crystallizing in equilibrium during this phase of the sequence, if local disequilibrium conditions were somehow obtained, then it might have been possible for the spinel to have survived the olivine-spinel-anorthite peritectic cooling phase. As a result, the spinel dunites together with newly crystallized anorthite could have formed spinel troctolites. The Mg′ of such spinel troctolites would be ~85, which, though lower than the maximum value for such rocks ($Mg'_{max} = 95$) is in the right range as reviewed in Section 5 of Paper II. However, due to the generally unlikely conditions needed to preserve the spinel, it seems rather doubtful that significant quantities of spinel troctolites could have been formed in this way. Also, the requirement that the crystallization path intersects the olivine-spinel cotectic means that, in addition to the spinel troctolites, all the early rocks would have to be olivine normative. This would be the case until the composition of the melt finally crossed the Alkemade line. This requirement is in direct conflict with the observation that the early anorthosites are frequently or generally quartz normative as discussed above. While it is possible that such a spinel troctolite phase of the cooling sequence was short lived and the melt composition moved rapidly to the quartz side of the Alkemade line, this possibility seems remote in the light of the above mentioned difficulty. Finally, as reviewed in Paper II, the weight of the evidence strongly

suggests that all or at least the greatest majority of the spinel troctolites are early cumulates formed during rapid, disequilibrium crystallization of impact melts. Thus, there seems to be little reason to consider this modification to the above discussed cotectic sequence, though this possibility can not be completely dismissed at this time.

6. The Distribution of U, Th and K in the Crust and Upper Mantle

A simple model for the distribution of U, Th and K (hereafter referred to collectively as UTK) is developed in Section 3 of Paper II and slightly modified in a later paper (Binder, 1975c, hereafter referred to as Paper III). The model is based on a mineral to liquid distribution coefficient (K) of 0.1 derived from data given by Rice and Bowie (1971) on the distribution of U in four Apollo 11 rocks. As will be shown, despite its simplicity, the model does quite accurately represent the distribution of UTK in the differentiated pyrolite Moon models. The following is, however, a much more rigorous treatment of the problem.

The simple model presented in Paper II was computed using the above mentioned K of 0.1 for all three major constituents of the Moon, i.e. olivine, pyroxene and plagioclase. As discussed in Paper III, this approximation is reasonable for pyroxenes in general and for plagioclase, but not for olivine. Comparisons of the concentrations of UTK in these three minerals found in terrestrial crustal rocks show that K for olivine is so low that UTK is almost completely excluded from the crystals. Thus, the model was slightly modified to take into account the absence of UTK in the dunite lower mantle of the Moon.

Similar comparisons of the concentrations of U in olivine, orthopyroxene and clinopyroxene in terrestrial ultramafic xenoliths (Kleeman *et al.*, 1969) from the mantle show that the distribution coefficient for olivine must be about 500 times lower than that for co-existing clinopyroxene. This result is consistent with, but even more restrictive than the one presented in Paper III. Likewise the concentration of U in orthopyroxene indicates that the distribution coefficient for orthopyroxene must be 100 to 150 times lower than for the co-existing clinopyroxene. Unfortunately, the ultramafic xenoliths studied by Kleeman *et al.* (1969) contain no plagioclase. Thus, this type of comparison can not be made between plagioclase and clinopyroxene. However, based on the data used in Paper III (i.e. Wedepohl, 1969), the concentration of UTK in plagioclase is about the same as in typical terrestrial pyroxenes, presumably clinopyroxenes. On the assumption that these observations hold for the anhydrus and very low f_{O_2} conditions of the lunar environment, then it is possible to obtain good estimates of K for olivine, orthopyroxene, clinopyroxene and plagioclase based on the value of K derived in Paper II.

The four Apollo rocks studied by Rice and Bowie (1971) contain about equal amounts of plagioclase and clinopyroxene (Schmitt *et al.*, 1970) and since the values of K for both minerals are about the same, the value of $K = 0.1$ derived from the data should be valid for both minerals. It then follows from the discussion above that $K = 0.001$ for orthopyroxene and $K = 0.0002$ for olivine. These values of K indicate that UTK is strongly excluded from orthopyroxene and nearly completely excluded from olivine. Thus, as was demonstrated in Paper III, the dunite lower mantle is

essentially free of UTK. Also, because of the low K for orthopyroxene, the concentration of UTK in the peridotite upper mantle is controlled by the ratio of clinopyroxene to orthopyroxene in the peridotite. From Gast (1968), the value of K for mixed phases is the weighted average of the individual values of K. According to the pyrolite models, the upper mantle consists of 10–20% olivine, 65–75% orthopyroxene and 10–20% clinopyroxene. From these data and the values of K derived above, the value of K for the peridotite is 0.01 to 0.02.

Now, in terms of the distribution of UTK in the Moon, there is no difference between the peritectic and cotectic sequences discussed above. The dunite lower mantle is almost completely free of UTK and the ortho-clinopyroxene plus olivine mixture, which formed the upper mantle, was equilibriated with the melt in both sequences. Thus, for the purposes of the UTK modeling, both differentiation schemes can be represented by the somewhat simpler peritectic sequence. A somewhat simplified system which quite accurately represents the lunar case is one in which, after the dunite lower mantle formed, pyroxene began to crystallize alone and in equilibrium with the melt. After some time, plagioclase began to co-crystallize with the pyroxene, but of course the plagioclase was removed from the system as it formed.

Now, the terms needed in the derivation of the equations used to define such a system are:

distribution coefficient for plagioclase	$K_a = 0.1$
distribution coefficient for pyroxene	$K_p = 0.001$–0.002
weight percent of remaining melt	f, $(1 \geq f \geq 0)$
weight percent of melt remaining when plagioclase begins to form	f_a
total amount of UTK in pyroxene	X_p
total amount of UTK in plagioclase	X_a
toatl amount of UTK in melt	X_1
mean concentration of UTK in melt	C.

Further, during the initial crystallization of such a system, when pyroxene alone forms, only two conditions need be met. First, the concentration of UTK in the pyroxene is uniform and is, by definition, K_p times the concentration (C) in the residual melt. Second, the total amounts of UTK in the pyroxene and melt is unity; thus,

$$X_p + X_1 = 1. \tag{18}$$

By definition,

$$X_p = K_p C(1 - f) \tag{19}$$

and

$$X_1 = Cf; \tag{20}$$

therefore,

$$C = (f - fK_p + K_p)^{-1}. \tag{21}$$

Equation (21) is valid for $1 \geq f \geq f_a$. Once the plagioclase begins to crystallize and is removed from the melt, the following three relationships hold. First, the total amounts of UTK in the plagioclase, pyroxene and melt is unity,

$$X_a + X_p + X_1 = 1. \tag{22}$$

Secondly, the instantaneous concentration $\left(\frac{dX_a}{df}\right)$ of UTK in the plagioclase is given by

$$\frac{dX_a}{df} = \frac{-K_a C}{2}. \tag{23}$$

The factor of 1/2 on the right side of equation (23) is due to the fact that 1/2 of the increment of melt (df) crystallizes as plagioclase and the other 1/2 crystallizes as pyroxene. Third, the total amount of UTK in the pyroxenes is given by

$$X_p = K_p C\left(\frac{2 - f_a - f}{2}\right), \tag{24}$$

where the factors $1 - f_a$ and $(f_a - f)/2$ in the parentheses are the amounts of pyroxene crystallized before and after plagioclase began to form, respectively. From Equations (20), (22) and (24) we have

$$X_a = 1 - \frac{C}{2}[K_p(2 - f_a) + f(2 - K_p)]. \tag{25}$$

Differentiating Equation (25) and using Equation (23) we have

$$\frac{2dX_a}{df} = -K_a C = -C(2 - K_p) - [K_p(2 - f_a) + f(2 - K_p)]\frac{dC}{df}. \tag{26}$$

By rearranging terms in Equation (26) we have

$$\frac{dC}{C} = \frac{(K_p - K_a - 2)df}{K_p(2 - f_a) + f(2 - K_p)}, \tag{27}$$

which by integration and simplification yields

$$C = A[K_p(2 - f_a) + f(2 - K_p)]\frac{(K_p - K_a - 2)}{(2 - K_p)}, \tag{28}$$

where A is the integration constant. Equation (28) is valid for $f_a \geq f \geq 0$. Together, Equations (21) and (28) give the concentration of UTK in the residual melt for the entire crystallization sequence for the crust and upper mantle of a pyrolite Moon. Once C is so defined, then the concentrations of UTK in the pyroxene and plagioclase are given by $K_p C$ and $K_a C$, respectively.

If we take the pyrolite M model as an example, the upper mantle-crust crystallization sequence started when 60% of the Moon had crystallized as olivine (and sank to form the lower mantle); hence, the concentration of UTK in the remaining 40% of the melt was 2.5 times the total concentration of these elements in the Moon. Pyroxene began to crystallize at that point and plagioclase began to form when 80% of the Moon had solidified. Normalizing the system so that $f = 1$ when pyroxene began to crystallize, then $f_a = 0.5$. From these quantities and Equation (28) one obtains the values (see Table VII) for the concentrations of UTK in the residual melt, in the equilibriated pyroxene and in the disequilibrium crystallized plagioclase. The data in Table VII are given in terms of the normalized f, the true f and for values of K_p of 0.01 and 0.02 as derived above.

TABLE VII

Normalized concentration of UTK in crust and upper mantle

Value of K_p		0.01			0.02		
f normalized	f real	C	$K_p C$	$K_a C$	C	$K_p C$	$K_a C$
1.00	0.40	2.50	0.025	—	2.50	0.050	—
0.75	0.30	3.32	0.033	—	3.31	0.033	—
0.50	0.20	4.95	0.050	0.50	4.90	0.098	0.49
0.40	0.16	6.10	0.061	0.61	6.02	0.120	0.60
0.30	0.12	7.97	0.080	0.80	7.82	0.156	0.78
0.20	0.08	11.57	0.116	1.16	11.23	0.225	1.12
0.10	0.04	21.61	0.216	2.16	20.33	0.407	2.03
0.04	0.016	46.92	0.469	4.69	40.90	0.818	4.09
0.02	0.008	78.80	0.788	7.88	62.73	1.255	6.27
0.00	0.000	269.8	2.698	2.70	139.5	2.790	14.00

The heavy line underlining the values of C etc. in Table VII indicate the point in the differentiation sequence where the concentration of UTK in the upper mantle yields the observed concentrations of UTK for the mare basalts at the appropriate degrees of partial melting (see Section 3 of Paper II). At that point, convection in the nearly completely solidified magmatic mush stopped. The residual fluid, which was high in UTK and KREEP elements, was confined to a thin zone between the newly formed crust and upper mantle, i.e. the KREEP zone discussed in papers I, II and III. The thickness of the KREEP layer depends on the value of K_p used and the concentration of UTK in the upper mantle. If, as is indicated by the mare basalt data, the concentration of UTK in the upper mantle is ~0.8 that of the whole Moon, then for $K_p = 0.01$ and 0.02 the KREEP layer is 5 and 10 km thick, respectively. These values compare favorably with the estimate of few km given for the thickness of the KREEP layer in Papers II and III. It is noted here that this

same terminal phase which is suggested for the formation of the KREEP layer (also see Papers I and II) was suggested earlier in Section 3 in order to explain the possible reversal of the differentiation trend suggested by the data given in Figure 4. It will be shown shortly that the UTK concentration in at least one of the rocks in the cluster at An_{92}, $Mg' = 70$ in Figure 4 is exactly that derived for the KREEP layer.

The model for the distribution of UTK in the pyrolite M Moon, as derived from the data in Table VII, is also given in Figure 15 along with the rock data given in Tables VIIIA and VIIIB of Paper II. Comparisons of the curves in Figure 15 with those given in Figure 5 of Paper II or Figure 1 of Paper III shows that the models are quite similar and that the mare basalt data are satisfied by all three models. In addition, the more refined model gives a value for the lunar heat flow of 13 to 14 ergs/cm^2/sec in accordance with the fission models as discussed in Paper III.

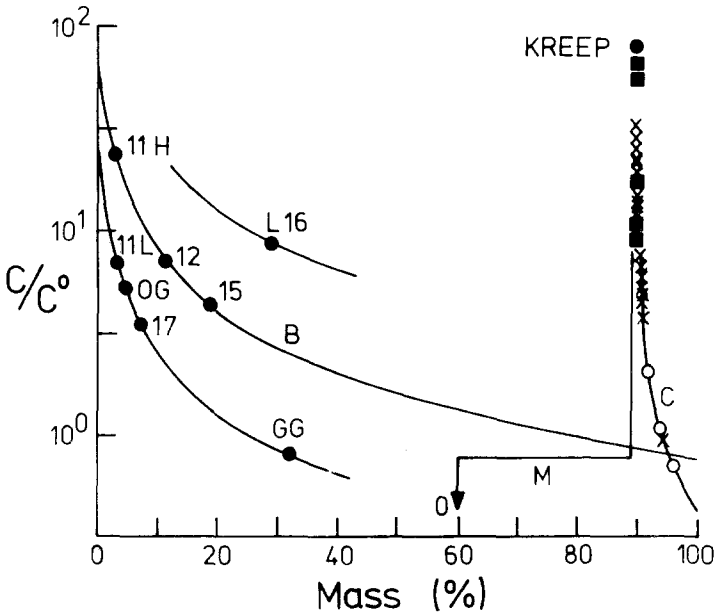

Fig. 15. Predicted concentration of UTK in a pyrolite M model Moon. The dunite lower mantle contains 60% of the mass of the Moon and lies between 0% and 60% mass in the figure; the peridotite upper mantle contains 30% of the mass and lies between 60% and 90% mass and the feldspathic crust contains 10% of the mass and lies between 90% and 100% mass. Curves M and C give the concentrations of UTK in the upper mantle and the crust, respectively, as given in Table VII. The KREEP point gives the concentration of UTK in the KREEP zone between the upper mantle and the crust. Curve B gives the concentrations of UTK in partial melts derived from the upper mantle. The short segments of curves above and below B give the concentrations of UTK in partial melts derived in areas within the upper mantle which have concentrations of UTK a factor of ± 3 that of the average upper mantle. The lunar rock data are taken from Tables VIIA and VIIB of paper II. The various mare basalts and the green (GG) and orange (OG) glasses are indicated by filled circles accompanied by an identification number and, in some cases, a letter. The highland rocks are indicated as follows: anorthosites by open circles, breccias by x's and crystalline rocks by filled squares. The x axis gives the mass of the Moon crystallized for curves M and C and the degree of partial melting for curves(s) B.

TABLE VIII

U and Th content for rocks in data base

Rock	U (ppm)	Th (ppm)	Reference
14066	4.1	15.3	LSPET, 1971
14310	3.7	13.7	
14315	2.5	9.1	
14318	3.3	12.8	
15415	0.0024	0.007	LSPET, 1972a
60016	0.51	2.10	Taylor *et al.*, 1974
61175	0.35	1.56	
64435	0.12	0.23	
67016	0.17	0.73	
68115	0.74	2.66	
60017	0.20	0.80	LSPET, 1972b
60315	2.34	8.56	
60335	0.92	2.75	
64435	0.03	0.10	
65015	3.00	10.00	
67115	0.12	0.43	
68415	0.35	1.22	
69935	0.62	2.52	
69955	0.04	0.14	
72275	1.7	6.7	Taylor *et al.*, 1974
73235 black	1.1	4.3	
73235 white	0.27	1.0	
76315 (mean)	1.51	5.7	Bence *et al.*, 1975
73215 matrix	1.3	5.3	
73215 clast	0.33	1.34	
77135	1.42	5.5	LSPET, 1973

While the model yields the correct concentrations of UTK for the mare basalts, the situation with the upland rocks is somewhat different. As was discussed briefly in Paper II, the upland rock data points generally lie about the computed curve for the crust and the mean concentration of UTK in the Apollo 16 and 17 upland samples is well above the mean for the model curve. This point is clearly illustrated in Figure 16 which gives the theoretical curve for the crust and the U + Th contents vs mafic contents of those rocks for which CIPW norms from the data base —and for which U and Th data are available (see Table VII). The crustal curve was derived taking into account the effects on the U + Th contents of the final rocks due to the trapping of melt (with high U + Th concentrations), pyroxene (low U + Th concentrations) and olivine (no U + Th), by the plagioclase crystals (intermediate concentrations of U and Th) using the data in Tables IIIB and VII and the Ol′ variations during crystallization used to derive the best fit curve in Figure 13.

As can be seen in Figure 16, the rock data lie everywhere above the computed crustal curve and the mean for the rock data is about 20 times higher than the model mean. However, it is noted that all the data points for the rocks with the highest U + Th contents lie about at the level predicted for the KREEP layer and that these rocks are mainly Apollo 14 rocks which are known to have come from depth in the crust. In addition, the rock denoted by the filled square is the afore mentioned rock which lies in the cluster at An_{92}, $Mg' = 70$ in Figure 4. These

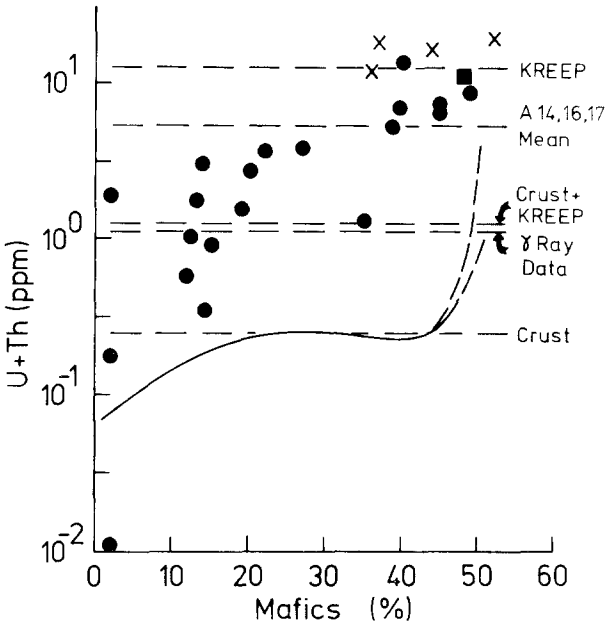

Fig. 16. Concentration of U + Th in upland rocks vs their mafic content. The X's represent the data for Apollo 14 rocks and the filled square represents the data for the rock discussed in the text. All five of these rocks are believed to have been excavated from the KREEP zone, whose calculated U + Th content is indicated by the upper dashed line. Filled circles give the data for all other types of upland rocks. The solid curve (with the two dashed branches) gives the computed U + Th content of the primitive suite of rocks; the lower dashed line gives the mean U + Th content of the crustal model. The dashed line designated by Crust + KREEP gives the mean U + Th content of the model lunar crust, when the KREEP materials are mixed with the crustal materials, see text. The dashed line designated by γ Ray Data gives the mean U + Th content of the crust as determined from orbital γ ray measurements. The dashed line designated by A14, 16, 17 Mean gives the mean U + Th content of the rocks returned as a result of the Apollo 14, 16 and 17 missions.

observations indicate that this rock and the Apollo 14 rocks most probably were excavated from the KREEP layer itself.

It is noted that almost all the points in Figure 16 lie between the mean level computed for the crust and the level determined for KREEP. Thus it appears that the concentration of UTK in the crust resulted from a mixing of the KREEP components with the primitive crustal rocks. It seems reasonable to assume that, due to excavation and upwards migration of the low melting components from the KREEP layer, KREEP, U and Th were disseminated throughout the crust during the first 5–6 $\times$ 10^8 years of lunar history (paper I) – i.e., during the intense early modification and metamorphism of the early crust.

However, there is no certain way of knowing how the KREEP components are distributed in a vertical column in the crust. For example, if the combined effects of impact excavation and upward migration of the low melting KREEP materials via metamorphic processes was not very efficient, then the amount of UTK in the rocks probably increases with depth in the crust. If so, then the surface rocks contain less UTK than does the average crust. However, if the upward migration of KREEP

fluids was very effective, then the amount of UTK in the crustal rocks decreases with depth and the surface rocks contain considerably more of these elements than does the average crust. Since there is, at present, no way of choosing between the models, it seems reasonable to assume that the truth lies somewhere between these two extremes and that the UTK is, on the average, uniformally mixed throughout a vertical column of the crust. Based on this assumption, the mean value for the concentration of U + Th in the average crust of the model is only a factor of 4 lower than that of the returned samples (see Figure 16).

A more global view of the situation can be gained from the γ ray spectrometer data of Metzger *et al.* (1974). Again assuming, that the UTK is uniformally mixed in a vertical column and hence that the orbital measurements give results which are representative of the entire crust, then the data given in Tables 3 and 4 of Metzger *et al.* (1974) for the highland regions show that the average crust contains 0.85 ppm of Th and 1000 ppm of K*. Using the well established Th/U ratio of 3.6 for lunar material, the concentration of Th given above indicates that the concentration of U in the average crust is 0.24 ppm. These values compare favorable with the values of U = 0.28 ppm, Th = 1.00 ppm and K = 800 ppm derived from the mixing model developed above based on a total content of U = 0.035 ppm, Th = 0.125 ppm and K = 100 ppm in the Moon (Paper III). Thus the orbital data indicate that the concentration of UTK in the crust is almost exactly that predicted by the pyrolite models. This result also indicates that the mean concentrations of UTK found in the Apollo 16 and 17 samples are 2 and 4 times higher than the global mean value. This finding tends to substantiate the model developed in Paper III which predicts that there are local (100–1000 km scale) variation in the KREEP-crustal concentration of UTK by at least a factor of 3 and that, as a result, the heat flow varies locally by at least a factor of 3.

Thus, the data and models indicate that the KREEP layer, which was formed at the end of the primary differentiation of the Moon, was a transient feature of the lunar interior. Due to the low melting point of its constituents and due to excavation by basin forming impacts, the KREEP components were intruded into and mixed with the primitive suite of crustal rocks early in lunar history. Based on this conclusion, the models show that today and for about the last 4×10^9 years of lunar history, the crust contains some 80% of the heat producing elements of the Moon and has a mean concentration of U = 0.28 ppm, Th = 1.00 ppm and K = 800 ppm. The remaining 20% of these elements are found in the upper mantle which has mean concentrations of U = 0.025 ppm, Th = 0.090 ppm and K = 70 ppm.

7. Conclusions

Based on the excellent match of the rock data with the predicted trends and boundaries of the upland rock model developed in Paper II and this paper, it appears that the model adequately describes the physical and chemical conditions

* It is noted that the crustal concentrations derived here using the γ ray data are a factor of 2 lower than those quoted by Taylor (1975) who used the same data, but apparently did not weight the data given by Metzger *et al.* (1974) according to area.

which existed in the outer part of the Moon when the upper mantle and crust developed. The major features of the primitive upland rocks accounted for by the model are (1) the decrease in An contents of the plagioclase of the rocks with increasing mafic content and hence, time of development in the sequence, (2) the reversed An vs Mg′ trend of the rocks and (3) the tendency for the early anorthosite rocks to be quarz normative. Also, based on the best fit crustal model, the Mg′ value of the upper mantle is found to be 75, a value which is in accordance with earlier estimates based on mare basalt experimental data.

It is found that the olivine content of the upland rocks is too high to be explained by the origional, peritectic model of the development of the crust and upper mantle. As such, a cotectic sequence, in which pyroxene was formed due to the reaction of sinking olivine with the melt at depths of 300 km and less, is developed. This model adequately accounts for the high amounts of olivine found in the upland rocks and the occurrence of troctolites among the primitive rocks. This model also provides a mechanism by which the magma, from which the crust and upper mantle formed, was set into convective motion after the dunite lower mantle had formed. This mechanism is simply the release of large quantities of heat by the exothermic reaction, olivine + quartz (in melt) → pyroxene, which occurred mainly in the lower parts of the magma mass.

The distribution of UTK in the crust, based on the refined distribution model developed in this paper and the proposal that the materials of early KREEP layer are uniformally mixed with the crustal rocks by metamorphism and impact excavation, is shown to give the same surface concentration of UTK as is derived from the orbital γ ray data. This point strengthens the arguments that the mean concentrations of U, Th and K in the Moon are basically the same as in the Earth's mantle and are about 0.035 ppm, 0.125 ppm and 100 ppm, respectively. This conclusion indicates that the mean heat flow of the Moon is 13–14 ergs/cm^2/sec and hence, that the Apollo heat flow measurements were made in areas with higher than average heat flow as discussed in an earlier paper.

While it is the case that the crustal developmental model presented can be applied to models other than the pyrolite fission models, the facts that (1) the differentiation scheme developed for the pyrolite models leads directly to the crustal developmental model both in terms of the physical conditions needed to drive the system and in terms of the composition of the magma, (2) the models developed are in accordance with the UKT data on the upland rocks and mare rocks and (3) the seismic evidence for the 300 km discontinuity, an En_{75} rich upper mantle and a Fo_{95} dominated total mantle (see Figure 13 of Dainty *et al.*, 1974) all strongly favor the fission origin of the Moon.

Acknowledgements

I would like to thank Dr Zschau for his help in developing the equations in Section 6 and both Dr Zschau and Professor Dr Meissner for their helpful discussions and criticisms of the models.

Addendum

As discussed in the main body of this paper, it is assumed that, on average, the majority of the present day upland rocks have retained the compositions of their parental rocks. As such, the rocks can be used to determine the compositional characteristics of the early primitive suite of upland rock. Only those rocks which clearly have undergone considerable compositional alteration, i.e. the spinel troctolites and possibly the melt rocks, were excluded from consideration in evaluating the models. Although, as is demonstrated in this addendum, it is possible to define reasonable selection rules for determining which rocks have really retained their parental compositions and which have not. Such a selection of the data was not made in the early development of the models as discussed in the main part of this paper. This was done for two reasons: first, it is the author's opinion that the reader should have a chance to evaluate the fit of the widest possible range of rock data to the models, despite the possibility that some of the data are marginal and thereby increase the scatter of the points in the various diagrams. If the models are valid, then there should be recognizable trends despite the scatter. Second, in the development of a model for a system as complicated as the crust of the moon, there is always the danger that the premature application of data selection rules will result in the loss of information which either contradicts the proposed model or which would lead to a refinement of the model – neither of which is desirable.

As is hopefully demonstrated to the reader earlier in this paper, the rocks of the data base do fit the proposed model quite well and therefore it seems reasonable to assume that selection rules can now be applied to the rock data. As is shown in the figures of this addendum, the result of this data selection procedure is simply that the scatter of the data points in the previously given figures is drastically reduced and that the data fit the various predicted boundaries and trends even better than before. None of the empirical curves derived from the data are substantially altered, nor are any of the conclusions derived from the fit of the data to the models. Hence, the following is simply a description of the selection rules and the plots derived from the selected data.

The first selection rule applies to the quartz normative rocks, principally anorthosites. As discussed in the text, the maximum amount of normative quartz and pyroxene in the peritectic or cotectic fluid is 6% and 43%, respectively. Thus, if a rock is primitive, the maximum amount of normative quartz which it could have would be about 0.14 times its normative pyroxene content. Of the 11 quartz normative anorthosites in the data base, 6 contain 2 to 5 times too much quartz to be primitive.

The second selection rule is related to the normative composition of the pyroxenes of the rocks. Figure A1 gives the composition of the pyroxenes of all the rocks in the data base. It is assumed that those rocks which have primitive compositions lie in the tight cluster of points within the ellipse. This criteria is somewhat relaxed for the anorthosites since the amounts of FeO, MgO and residual CaO (after the majority of the CaO has gone into anorthite) are so small that the uncertainties in their measurement are large fractions of their measured values. Hence,

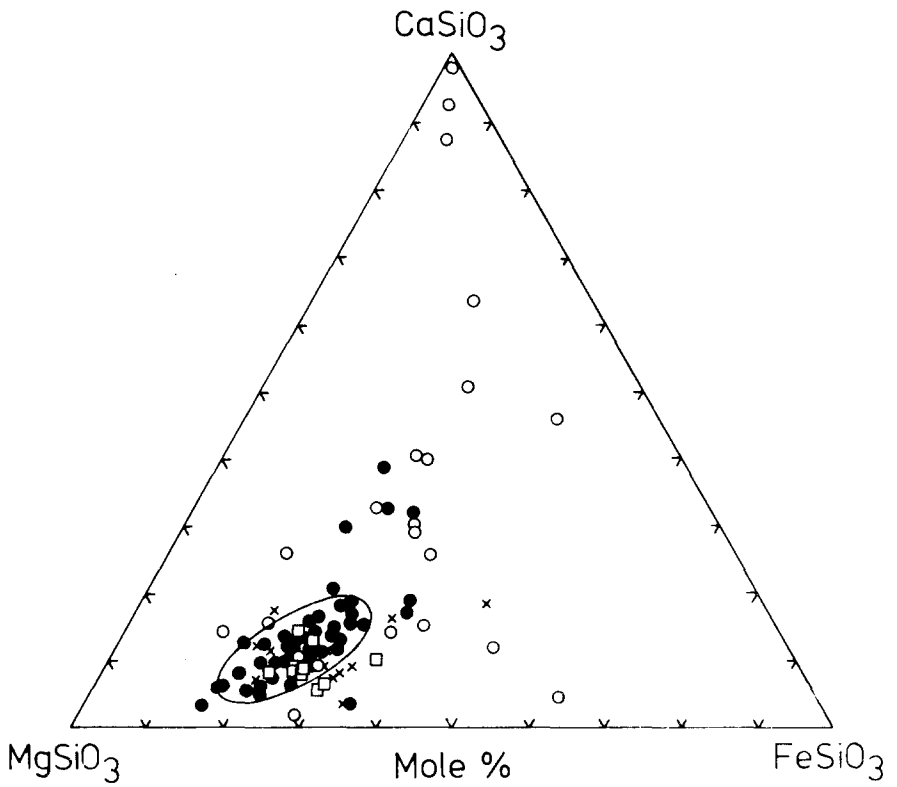

Fig. A1. CIPW norm compositions of the pyroxenes in the rocks of the data base. The rock symbols are the same as in Figure 4. The rocks whose compositions are thought to be primitive lie in the tight cluster of points encircled by the ellipse.

the anorthites (6) which plot within 10 mole % of the ellipse are not excluded by at least this selection rule.

The third selection rule is based on the normative composition of the plagioclase of the rock as is shown in Figure A2. Rocks with primitive compositions are assumed to lie between the two lines bordering the majority of the points.

It is almost invariably the case that rocks which fail to pass one of the tests also fail to pass at least one of both of the others. For example, the six quartz normative anorthosites which were rejected because they contained too much quartz all lie outside the extended pyroxene ellipse and one is also rejected by the plagioclase selection rule. In addition all of the ferroan anorthosites with $Mg' = 45$, which lie to the left of the model boundary in Figure 4, are among the rocks rejected based on the criteria. (Hence as suggested in Paper II, these rocks are certainly of secondary origin.) Other examples include the three poiklitic rocks (open squares) and three Apollo 14 rocks (X's) which lie just to the right and below the ellipse in Figure A1. The same rocks lie above (in one case on) the upper plagioclase boundary in Figure A2.

As mentioned above and in the text, it is assumed that melt rocks (Dowty *et al.*, 1974b) might not have primitive compositions and as such were excluded from

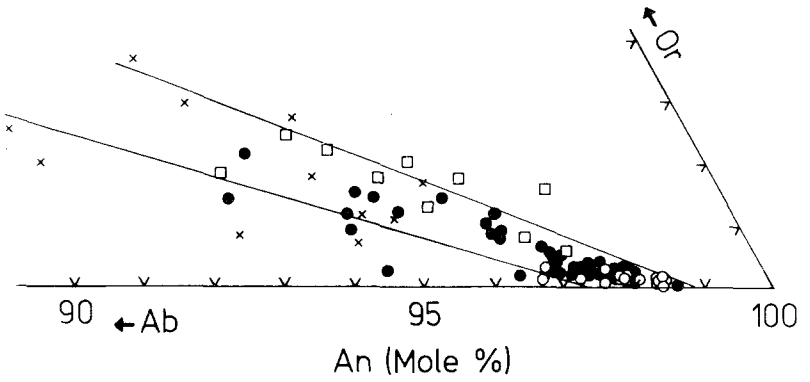

Fig. A2. CIPW norm compositions of the plagioclase in the rocks of the data base. The rock symbols are the same as in Figure 4. The rocks whose compositions are thought to be primitive lie within the two lines.

the data base. The validity of the assumption is demonstrated by noting that of the six melt rocks listed in Dowty *et al.*'s Table I, only one passes the selection criteria. Thus, in general, melt rocks are not primitive in the sense used in this paper.

When these selection rules are applied to all the rocks in the data base, about 50 of the some 100 rocks are found to have primitive compositions. These 50 rock points are plotted in Figures A3 and A4 which can be directly compared with Figures 6 and 4, respectively, in the main text. Such a comparison shows that the

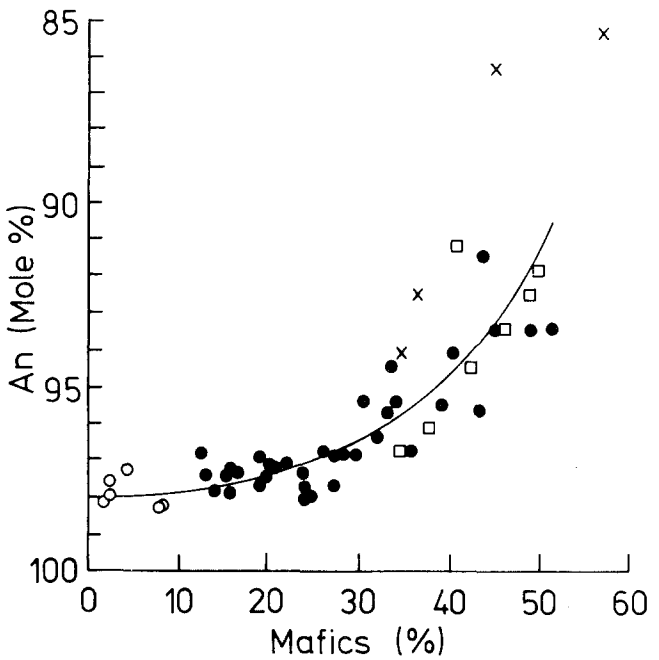

Fig. A3. An contents of the plagioclase vs the mafic contents of the primitive rocks definition Figures A1 and A2 and in the addendum text. The rock symbols are the same as in Figure 4.

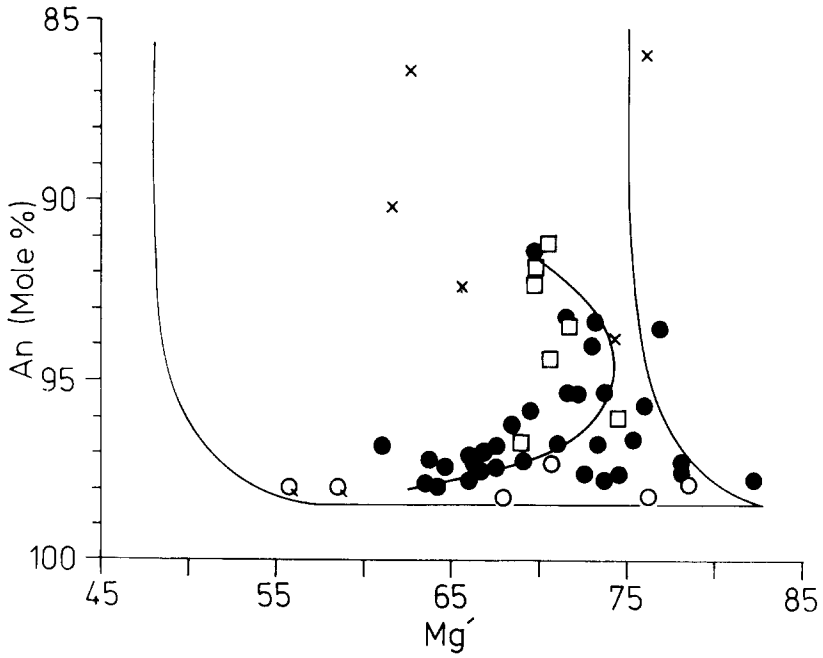

Fig. A4. An contents of the plagioclase vs the Mg′ contents of the primitive rocks defined in Figures A1 and A2 and in the addendum text. The boundary curves and the rock symbols are the same as in Figure 4. The curve through the rock points gives the mean An vs Mg′ composition of the rocks.

scatter of the data points in Figures 4 and 6 are considerably reduced as a result of the application of these selection criteria to the data and that the selected data fit the model in Figure A4, within the errors of the points, exactly. This is also true for Figures 5 and 14, which are not reproduced here. In particular among the points excluded in Figure 5 are the 10–15% point lying below the 0% limiting curve in the lower diagram and the two 20–25% points lying below the 20% curve in the middle diagram. Similarly, among the points excluded in Figure 14 are the two anorthosite points at Mg′ = 61 and 72. Thus, in all cases, the filtering of the data leads to a more exact fit of the points within the predicted boundaries and along the predicted trends of the crustal developmental model.

References

Bence, A. E., Taylor, S. R., Muir, P. M., Nance, W. B., Rudowski, R., and Ware, N.: (1975) in *Lunar Science* **VI**, The Lunar Science Institute, Houston, p. 36.

Biggar, G. M., O'Hare, M. J., Peckett, A., and Humphries, D. J.: 1971, *Proc. Second Lunar Sci. Conf.* **1**, 617.

Binder, A. B.: 1974a, abstract, in *Lunar Science* **V**, The Lunar Science Institute, Houston, p. 63.

Binder, A. B.: 1974b, *The Moon* **11**, 53.

Binder, A. B.: 1975a, abstract, in *Lunar Science* **VI**, The Lunar Science Institute, Houston, p. 54.

Binder, A. B.: 1975b, *The Moon* **13**, 431.

Binder, A. B.: 1975c, *The Moon* **14**, 237.

Chao, E. C. T. and Minkin, J. A.: 1975 in *Lunar Science* **V**, The Lunar Science Institute, Houston, p. 109.
Dainty, A. M., Toksöz, M. N., Solomon, S. C., Anderson, K. R., and Goins, N. R.: 1974, *Proc. Fifth Lunar Sci. Conf.* **3**, 3091.
Dowty, E., Keil, K., and Prinz, M.: 1972, in *The Apollo 15 Samples*, The Lunar Science Institute, Houston, p. 62.
Dowty, E., Keil, K., and Prinz, M.: 1974a, *Proc. Fifth Lunar Sci. Conf.* **1**, 431.
Dowty, E., Prinz, M., and Keil, K.: 1974b, *Earth Planet. Sci. Lett.* **24**, 15.
Duncan, A. R., Erlank, A. J., Willis, J. P., and Ahres, L. H.: 1973, *Proc. Fourth Lunar Sci. Conf.* **3**, 1097.
European Consortium: 1974, in *Lunar Science* **V**, The Lunar Science Institute, Houston, p. 215.
Gast, P. W.: 1968, *Geochim. Cosmochim. Acta* **32**, 1057.
Green, D. H. and Ringwood, A. E.: 1972, in *The Apollo 15 Lunar Samples*, The Lunar Science Institute, Houston, p. 82.
Green, D. H. and Ringwood, A. E.: 1973, *Earth Planet. Sci. Lett.* **19**, 1.
Green, D. H., Ringwood, A. E., Ware, N. G., and Hibberson, W. O.: 1972, *Proc. Third Lunar Sci. Conf.* **3**, 197.
Green, D. H., Ringwood, A. E., Ware, N. G., Hibberson, W. O., Major, A., and Kiss, E.: 1971, *Proc. Second Lunar Sci. Conf.* **1**, 601
Grieve, R. A. F., Plant, A. G., and Dence, M. R.: 1974, *Proc. Fifth Lunar Sci. Conf.* **2**, 261.
Hubbard, N. J., Rhodes, J. M., Gust, P. W., Bansal, B. M., Shih, C. Y., Wiesmann, H., and Nyquist, L. E.: 1973, *Proc. Fourth Lunar Sci. Conf.* **2**, 1297.
Hubbard, N. J., Rhodes, M. J., Wiesmann, H., Shih, C. Y., and Bansal, B. M.: 1974, *Proc. Fifth Lunar Sci. Conf.* **2**, 1227.
Kaula, W. M., Schubert, G., Lingenfelter, R. E., Sjogren, W. L. and Wollenhaupt, W. R.: 1974, *Proc. Fifth Lunar Sci. Conf.* **3**, 3049.
Kleeman, J. D., Green, D. H. and Lovering, J. F.: 1969, *Earth Planet. Sci. Lett.* **5**, 449.
Kushiro, I.: 1972, in *The Apollo 15 Lunar Samples*, The Lunar Science Institute, Houston, p. 128.
Kushiro, I., Nakamura, Y., Kitayama, K. and Akimoto, S.: 1971, *Proc. Second Lunar Sci. Conf.* **1**, 481.
Longhi, J., Walker, D., Grove, T. L., Stolper, E. M. and Hays, J. F.: 1974, *Proc. Fifth Lunar Sci. Conf.* **1**, 447.
LSPET: 1971, *Science*, **173**, 681.
LSPET: 1972a, *Science*, **175**, 363.
LSPET: 1972b, in 'Apollo 16 Preliminary Science Report', NASA, Wash. D. C., Sec. 7.
LSPET: 1973, in 'Apollo 17 Preliminary Science Report', NASA, Wash. D.C., Sec. 7.
Metzger, A. E., Tronblea, J. I., Reedy, R. C., and Arnold, J. R.: 1974, *Proc. Fifth Lunar Sci. Conf.* **2**, 1067.
Nakamura, Y., Latham, G., Lammlein, M. E., Duennebier, F. and Dorman, J.: 1974, *Geophys. Res. Letters* **1**, 137.
Prinz, M., Dowty, E., Keil, K. and Bunch, T. E.: 1973a, *Science*, **179**, 74.
Prinz, M., Dowty, E., Keil, K. and Bunch, T. E.: 1973b, *Geochim. Cosmochim. Acta* **37**, 979.
Ringwood, A. E.: 1975, abstract, in *Lunar Science* **VI**, The Lunar Science Institute, Houston, p. 674.
Ringwood, A. E. and Essene, E.: 1970, *Science*, **167**, 607.
Rice, C. M. and Bowie, S. H. V.: 1971, *Proc. Second Lunar Sci. Conf.* **1**, 159.
Roeder, P. L. and Emslie, R. F.: 1970, *Contr. Mineral. Petrol.* **29**, 275.
Rose, H. J., Jr., Cuttitta, F., Annell, C. S., Carron, M. K., Christian, R. P., Dwornik, E. J., Greenland, L. P., and Ligon, D. T., Jr.: 1972, *Proc. Third Lunar Sci. Conf.* **2**, 1215.
Rose, H. J., Jr., Cuttitta, F., Berman, S., Carron, M. K., Christian, R. P., Dwornik, E. J., Greenland, L. P., and Ligon, D. T., Jr.: 1973, *Proc. Fourth Lunar Sci. Conf.* **2**, 1149.
Schmitt, H. H., Lofgren, G., Swann, G. A. and Simmons, G.: 1970, *Proc. Apollo 17 Lunar Sci. Conf.* **1**, 1.
Steele, I. M. and Smith, J. V.: 1973, *Proc. Fourth Lunar Sci. Conf.* **1**, 519.
Stoeser, D. B., Wolfe, R. W., Marvin, U. B., Wood, J. A. and Bower, J. F.: 1974a in *Lunar Science* **V**, The Lunar Science Institute, Houston, p. 743.
Stoeser, D. B., Marvin, U. B., Wood, J. A., Wolfe, R. W. and Bower, J. F.: 1974b, *Proc. Fifth Lunar Sci. Conf.* **1**, 355.
Taylor, R. S.: 1975, *Lunar Science: A Post Apollo View*, Pergamon Press, Inc., N.Y., pp. 221, 231, 233, 245, 253.
Taylor, S. R., Gorton, M., Muir, P., Nance, W., Rudowski, R., and Ware, N.: 1974, in *Lunar Science* **V**, The Lunar Science Institute, Houston, p. 789.
Walker, D., Longhi, J., and Hays, J. F.: 1972, *Proc. Third Lunar Sci. Conf.* **1**, 797.
Walker, D., Longhi, J., Grove, T. L., Stolper, E., and Hays, J. F.: 1973, *Proc. Fourth Lunar Sci. Conf.* **1**, 1013.

Walker, D., Longhi, J., and Hays, J. F.: 1975, abstract, in *Lunar Science* **VI**, The Lunar Science Institute, Houston, p. 838.
Warner, J. L., Simonds, G. H., and Phinney, W. C.: 1974, *Proc. Fifth Lunar Sci. Conf.* **1**, 379.
Weill, D. F. and McKay, G. A.: 1975, in *Lunar Science* **VI**, The Lunar Science Institute, Houston, p. 863.
Wedepohl, K. H., ed.: 1969, *Handbook of Geochemistry*, Vol. II/2, Springer-Verlag, Berlin, sec. 19.
Weinrebe, W., Voss, J., and Meissner, R.: 1976, *Geologischen Jahrbuch*, Reihe E7, in press.
Wood, J. A.: 1975a, abstract, in *Lunar Science* **VI**, The Lunar Science Institute, Houston, p. 881.
Wood, J. A.: 1975b, Proc. Sixth Lunar Sci. Conf., *Geochim. Cosmochim. Acta*, in press.